

Intermediate-mass star models with different helium and metal contents

Giuseppe Bono¹, Filippina Caputo¹, Santi Cassisi^{2,3}, Marcella Marconi⁴, Luciano Piersanti^{2,5}, and Amedeo Tornambè²

Received _____; accepted _____

¹Osservatorio Astronomico di Roma, Via Frascati 33, 00040 Monte Porzio Catone, Italy; bono@coma.mporzio.astro.it, caputo@coma.mporzio.astro.it

²Osservatorio Astronomico di Collurania, Via M. Maggini, 64100 Teramo, Italy; cassisi@astrte.te.astro.it, tornambe@astrte.te.astro.it

³Max-Planck-Institut für Astrophysik, Karl-Schwarzschild-Strasse 1, 85740 Garching bei München, Germany

⁴Osservatorio Astronomico di Capodimonte, Via Moiariello 16, 80131 Napoli, Italy; marcella@na.astro.it

⁵Università di Napoli, Dip. di Fisica, 80131 Napoli, Italy; piersanti@astrte.te.astro.it

ABSTRACT

We present a comprehensive theoretical investigation of the evolutionary properties of intermediate-mass stars. The evolutionary sequences were computed from the Zero Age Main Sequence up to the central He exhaustion and often up to the phases which precede the carbon ignition or to the reignition of the H-shell which marks the beginning of the thermal pulse phase. The evolutionary tracks were constructed by adopting a wide range of stellar masses ($3 \leq M/M_{\odot} \leq 15$) and chemical compositions. In order to account for current uncertainties on the He to heavy elements enrichment ratio ($\Delta Y/\Delta Z$), the stellar models were computed by adopting at $Z=0.02$ two different He contents ($Y=0.27, 0.289$) and at $Z=0.04$ three different He contents ($Y=0.29, 0.34$, and 0.37). Moreover, to supply a homogeneous evolutionary scenario which accounts for young Magellanic stellar systems the calculations were also extended toward lower metallicities ($Z=0.004, Z=0.01$), by adopting different initial He abundances.

We evaluated for both solar ($Z=0.02$) and super-metal-rich (SMR, $Z=0.04$) models the transition mass M^{up} between the stellar structures igniting carbon and those which develop a full electron degeneracy inside the carbon-oxygen core. We found that M^{up} is of the order of $7.7 \pm 0.5M_{\odot}$ for solar composition, while for SMR structures an increase in the He content causes a decrease in M^{up} , and indeed it changes from $9.5 \pm 0.5M_{\odot}$ at $Y=0.29$, to $8.7 \pm 0.2M_{\odot}$ at $Y=0.34$, and to $7.7 \pm 0.2M_{\odot}$ at $Y=0.37$. We also show that M^{up} presents a nonlinear behavior with metallicity, and indeed it decreases when moving from $Z=0.04$ to $Z \approx 0.001$ and increases at lower metal contents. This finding confirms the predictions by Cassisi & Castellani (1993) and more recently by Umeda et al. (1999) and suggests that the rate of SNe type Ia depends on the

chemical composition of the parent stellar population.

This approach allows us to investigate in detail the evolutionary properties of classical Cepheids. In particular, we find that the range of stellar masses which perform the blue loop during the central He-burning phase narrows when moving toward metal-rich and SMR structures. This evidence and the substantial decrease in the evolutionary time spent by these structures inside the instability strip bring out that the probability to detect long-period Cepheids in SMR stellar systems is substantially smaller than in more metal-poor systems.

Moreover and even more importantly, we find that the time spent by Cepheids along the subsequent crossings of the instability strip also depends on the stellar mass. In fact, our models suggest that low-mass, metal-poor Cepheids spend a substantial portion of their lifetime along the blueward excursion of the blue loop, while at higher masses ($M/M_{\odot} \geq 8$) the time spent along the redward excursion becomes longer. Models at solar chemical composition present an opposite behavior i.e. the time spent along the redward excursion is longer than the blueward excursion among low-mass Cepheids and vice versa for high-mass Cepheids. Oddly enough, the time spent along the blueward excursion is for models at $Z=0.01$ longer than the redward excursion over the entire mass range. This suggests a nonlinear dependence of crossing times on metallicity. The time spent along the first crossing of the instability strip is generally negligible with the exception of high-mass, metal-poor stellar structures for which it becomes of the order of 15-20% of the total crossing time.

Subject headings: stars: early-type – evolution – intermediate mass – oscillations – variables: Cepheids, other

1. Introduction

A great deal of theoretical and observational studies have been recently devoted to the evolutionary and pulsational properties of metal-rich stellar structures. Thanks to the new radiative opacities (Seaton et al. 1994; Iglesias & Rogers 1996, and references therein), it has been possible to investigate on appropriate physical bases the evolutionary properties of metal-rich and SMR stellar populations (Stothers & Chin 1993, hereinafter SC93; Bressan, Chiosi, & Fagotto 1994; Weiss, Peletier, & Matteucci 1995; Bertelli et al. 1996; Salasnich et al. 1999; Girardi et al. 2000). Within this context Bono et al. (1997a,b,c) investigated the evolutionary properties of metal-rich, and SMR low-mass stars from the central H-burning up to the cooling sequence of white dwarfs, and provided a comprehensive theoretical scenario to account for the pulsation behavior of He-burning radial variables.

The main aim of this paper is to extend Bono et al. (1997a,b,c) theoretical framework to intermediate-mass stars, i.e. to those stars which after burning H and He eventually form carbon-oxygen (CO) cores under strong electron degeneracy conditions. Due to the occurrence of mass loss, these stars end up their evolution as CO white dwarfs. Several empirical and theoretical arguments seem to support the evidence that CO white dwarfs belonging to close binary degenerate stars (Iben & Livio 1993) become SNe type Ia progenitors. More massive stars succeed in igniting carbon, since they are marginally affected by electronic degeneracy, and therefore their final fate is to plausibly become the progenitor of core-collapse supernovae.

Dating back to the pioneering investigation by Alcock & Paczyński (1978), the evolutionary behavior of intermediate and moderately high-mass stars has been thoroughly investigated (Becker & Iben 1981; Castellani, Chieffi & Tornambé 1983; Maeder & Meynet 1987; Castellani, Chieffi, & Straniero 1990, hereinafter CCS; Lattanzio 1991; Bressan et al. 1993; Cassisi et al. 1994; Meynet et al. 1994; Castellani et al. 1999). However, the

large majority of these predictions are based on old radiative opacities or typically adopt a single value of the He to metal enrichment ratio. In order to account for the dependence of intermediate-mass stars on this parameter, present calculations are performed by adopting for each metal abundance two or three different He contents, as well as the most up-to-date input physics.

This theoretical framework will be adopted for discussing the evolutionary properties of two groups of variable stars, namely β Cephei stars⁶ and classical Cepheids. The reasons why we are interested in these variables is twofold:

1) during the last few years the observational properties of β Cephei stars have been substantially improved thanks to the high quality multiband Strömberg CCD data of young open clusters (Balona 1994; Balona & Laney 1995). These new data play a pivotal role for providing reliable evaluations of both the distance modulus and the reddening of the parent cluster. At the same time, they also provide suitable constraints on the physical parameters which govern the evolutionary and pulsational properties of β Cephei stars. This occurrence makes β Cephei stars a useful benchmark for testing the observables predicted by pulsation and evolutionary theories for young, early-type stars.

Detailed theoretical investigation on the evolutionary and pulsation properties of β Cephei stars have been provided by Balona, Dziembowski, & Pamyatnykh (1997) and more recently by Pamyatnykh (1999). The evolutionary tracks presented by these authors were constructed by adopting fixed He abundance ($Y=0.28$) and two different metal contents, namely $Z=0.02$ and $Z=0.03$. However, empirical evidence based on spectroscopic

⁶ β Cephei stars are a group of early-type B pulsating stars characterized by periods of the order of few hours, luminosity amplitudes which range from few hundredths to few tenths of magnitude and velocity amplitudes of few tens of km/sec.

measurements (Waelkens, Van den Abeele, & Van Winckel 1991) suggest that the instability strip of these objects depends on metallicity. This finding was soundly confirmed by Gies & Lambert (1992) on the basis of high signal-to-noise Reticon spectra of 31 field, B-type, giant stars. In fact, they found that the mean metallicity of their sample is of the order of $Z=0.035$ which means, without invoking error bars that the mean metallicity of field, early B-type stars is almost a factor of two larger than the solar metallicity. It is interesting to note that in the sample investigated by Gies & Lambert are included 10 β Cephei stars and among them only two objects (ξ^1 CMa, PT Pup) are more metal-poor than the mean, whereas the other are more metal-rich than the mean. As a consequence, we are interested in implementing current evolutionary predictions with SMR structures. Linear, nonadiabatic pulsation properties of β Cephei stars will be addressed in a companion paper.

2) Classical Cepheids are the most popular standard candles for estimating cosmic distances and recent full amplitude, nonlinear, convective models (Bono, Marconi, & Stellingwerf 1999a; Bono et al. 1999b; Bono, Castellani, & Marconi 2000) suggest that at fixed period metal-poor Cepheids are on average brighter than metal-rich ones. On the other hand, linear models and some observational estimates seem to suggest that the metallicity dependence is either negligible (Gieren, Fouqu e, & Gomez 1998; Alibert et al. 1999, hereinafter ABHA) or at variance with nonlinear predictions (Sasselov et al. 1997; Kennicutt et al. 1998). This conundrum is still unsettled, but very recent empirical evidence suggest that Cepheid properties do depend on metallicity (Paczynski & Pindor 2000) and that at fixed period Galactic Cepheids maybe fainter than LMC Cepheids (Groenewegen & Oudmaijer 2000). Theoretical predictions based on both linear and nonlinear pulsation models rely on the Mass-Luminosity (ML) relation predicted by evolutionary models. To test the reliability of current ML relations the evolutionary framework developed in the present investigation will be used to evaluate the dependence of the ML relation on both He and metal abundances. Moreover in order to estimate the intrinsic spread in luminosity,

at fixed stellar mass, we supply a detailed analysis of the time spent inside the instability strip during the subsequent crossings of the pulsation region.

The paper is organized as follows. In §2 we briefly discuss the theoretical framework adopted for constructing the evolutionary models, together with the selected chemical compositions. The main properties of the stellar evolution models are detailed in §3; H and He-burning phases are discussed in sections 3.1 and 3.2, while the dependence of the evolutionary behavior on mass loss and on $^{12}\text{C}(\alpha, \gamma)^{16}\text{O}$ nuclear reaction rate is presented in §3.3. The effects of chemical composition on M^{up} are discussed in §3.4. Finally, the dependence of evolutionary time spent inside the Cepheid instability strip on chemical composition are presented in §4, together with the new ML relation. The main results of this investigation are summarized in §5. In this section we briefly outline the observables which can help to validate the current evolutionary scenario.

2. Theoretical Stellar Models

Theoretical stellar models have been computed using the FRANEC (Straniero & Chieffi 1989; Cassisi & Salaris 1997; Castellani et al. 1997) evolutionary code. The OPAL radiative opacities (Iglesias & Rogers 1996) are adopted for temperatures higher than 10,000 K, while for lower temperatures we use the molecular opacities by Alexander & Ferguson (1994). Both high and low-temperature opacities assume a solar scaled heavy element distribution (Grevesse 1991). The equation of state provided by Straniero (1988) is supplemented at lower temperatures with a Saha EOS, and the outer boundary conditions are fixed according to the $T(\tau)$ relation by Krishna-Swamy (1966). In the outer layers the superadiabatic convection is treated by means of the canonical mixing length - ml -formalism. We adopt a ml parameter which scales with the metallicity, i.e. $ml=2.2$ for $Z \geq 0.01$, and $ml=1.81$ for $Z=0.004$. The evolutionary models at solar metallicity ($Z=0.02$)

are constructed by adopting two initial He abundances, namely $Y=0.27$, and $Y=0.289$. The latter value is obtained by calibrating the present sun with a non-diffusive solar standard model (Salaris & Cassisi 1996, hereinafter SC).

It is worth mentioning that these values are in good agreement with recent spectroscopic measurements of M17 -a bright Galactic HII region- by Esteban et al. (1999) who found $Y= 0.280 \pm 0.006$. To fix the chemical composition of the SMR Zero Age Main Sequence (ZAMS) models, a suitable assumption on the value of the $\Delta Y/\Delta Z$ parameter has to be provided as well. However, the value of this parameter is a thorny problem (Zoccali et al. 2000, and references therein), since current estimates are still affected by large uncertainties. Empirical evaluations range from $\Delta Y/\Delta Z \approx 6$ (Pagel et al. 1992) to $\Delta Y/\Delta Z = 2.17 \pm 0.4$ (Peimbert, Peimbert, & Ruiz 2000), while chemical evolution models seem to suggest a $\Delta Y/\Delta Z$ value equal to 1.6 for the solar neighborhood (Chiappini, Matteucci, & Gratton 1997), and a very similar value ($\Delta Y/\Delta Z=1.7$) for irregular galaxies (Carigi, Colin & Peimbert 1999). Moreover, recent evaluations of the He abundance in the Galactic bulge (Renzini 1994; Bertelli et al. 1996) also suggest a He abundance ranging from $Y=0.25$ to 0.35. On the basis of these evidence, we adopt $Y=0.34$ ($\Delta Y/\Delta Z=2.8$) as a plausible assumption for the original He content of SMR stellar models ($Z=0.04$). However, to account for current uncertainties, we also compute two new sets of evolutionary tracks by adopting $Y=0.29$ ($\Delta Y/\Delta Z=1.5$) and $Y=0.37$ ($\Delta Y/\Delta Z=3.5$).

In order to supply an evolutionary framework which covers the metallicity range of young stellar clusters and Cepheids in the Magellanic Clouds (MCs) we constructed two sets of evolutionary models with $Z=0.01$ and $Z=0.004$ (Luck et al. 1998). For the former metallicity, which is representative of the Large Magellanic Cloud (LMC), we adopt three different initial He contents, namely $Y=0.23$, 0.255, 0.27, while for the latter, which is representative of the Small Magellanic Cloud (SMC), we adopt $Y=0.23$ and $Y=0.27$. We

note that current empirical estimates suggest for the SMC a He content of the order of $Y=0.24$ (Peimbert & Peimbert 2000). To properly cover the range of stellar masses which perform a "blue loop" in the HR diagram, the evolutionary models are constructed by adopting a fine mass resolution. The evolution is followed from the ZAMS up to the central He exhaustion and often up to the phases which precede carbon ignition or to the reignition of the H shell which marks the start of the thermal pulse phase.

Theoretical predictions on the evolutionary behavior of intermediate and high-mass stars are still hampered by the treatment adopted to estimate, during central H-burning phase, the convective core overshooting beyond the formal boundary of the convective unstable region. Several theoretical and observational investigations have been focused on the evaluation of the efficiency of this mechanism in real stars (Chiosi et al. 1989; Chiosi, Bertelli & Bressan 1992). The present theoretical scenario seems to suggest that its efficiency could be low (Stothers & Chin 1992), and therefore we fix the boundary of the convective core according to the canonical Schwarzschild criterion. The evolution of massive stars depends also on the method adopted for treating the semiconvective layers which develop around the H core close to the H exhaustion. In fact, as originally suggested by Schwarzschild & Härm (1958) and Sakashita & Hayashi (1959), the occurrence of such a phenomenon is mainly due to the electron scattering opacity and to the large radiative flux. Outside the Schwarzschild boundary of the convective core, a portion of the H-rich envelope becomes convectively unstable, but if the core grows, the external layers are again brought back to stability. As a consequence, a zone of partial mixing is established where the nuclear processed material is mixed with the H-rich layers until stability is achieved.

Even though the effects of the Schwarzschild and the Ledoux criteria on the evolutionary behavior of massive stars is still debated (Brocato & Castellani 1993; Stothers & Chin 1994; Canuto 2000, and references therein), we adopted the former one, since the stability

criterion has a marginal effect on stellar models ranging from 3 to 12 M_{\odot} . At the same time, the evolutionary properties of intermediate and high-mass stars crucially depend on the $^{12}\text{C}(\alpha, \gamma)^{16}\text{O}$ nuclear reaction rate, and indeed the central He burning lifetime (Chin & Stothers 1991; Cassisi et al. 1998), the carbon/oxygen ratio -C/O- and the carbon/oxygen core mass (M_{CO}) at the central He exhaustion (Salaris et al. 1997; Umeda et al. 1999) are affected by this parameter. Although this nuclear reaction rate could be somehow constrained on the basis of the nuclear yields in massive stars (Thielemann, Nomoto & Hashimoto 1996), our knowledge of this rate is quite poor due to the current uncertainties in chemical evolution models, in massive star nucleosynthesis, and in the physical mechanisms which trigger the SNe explosion. In the present work, we adopt the rate for the $^{12}\text{C}(\alpha, \gamma)^{16}\text{O}$ derived by Caughlan et al. (1985, hereinafter CFHZ85). However, in order to estimate the dependence of the stellar properties on this parameter we computed selected evolutionary tracks by adopting the rate suggested by Caughlan & Fowler (1988, hereinafter CF88).

The evolutionary properties of massive stars are also affected by the efficiency of mass loss. The reader interested in the evolutionary effects of mass loss is referred to the thorough review by Chiosi & Maeder (1986) and more recently by Salasnich et al. (1999). The physical mechanisms which govern the mass loss in red objects and in particular its dependence on metal content are not well understood yet. A self-consistent theoretical approach for evaluating the mass loss rates has been recently suggested by Schaerer et al. (1996) who constructed a set of evolutionary models which include a proper treatment of the radiative transport equation in the outermost layers. Even though this theoretical framework seems to account for the mass loss rates in the blue region of the HR diagram, we still lack useful insights into the dependence of mass loss on metal content in low temperature objects. As a consequence, in the present investigation the mass loss is neglected, but to account for its effect on the evolutionary behavior we construct selected sequences by including various semi-empirical rates available in the literature.

3. Evolutionary Properties

The main evolutionary properties of intermediate and high-mass stellar models have been extensively discussed in the literature (see §1), and in this section we address in more detail the properties of metal-rich and SMR models ($Z=0.04$) and the dependence on the initial He abundance. Tables 1-4 list selected evolutionary parameters for both H and He burning phases. Columns (1) to (9) give: the stellar mass, the mass of the convective core at the beginning of the H-burning phase (M_{cc}^H), the mass of the He core at the exhaustion of central H (M_{He}^H), the central H-burning lifetime (τ_H), the He core mass at the beginning of the central He-burning (M_{He}^{He}), the mass of the convective core at the same evolutionary phase (M_{cc}^{He}), the mass of the He core (M_{He}) and of the CO core (M_{CO}) at the exhaustion of central He, the central He-burning lifetime (τ_{He}). Columns (10) and (11) list the mass of the CO core and the surface luminosity at the second dredge up, while in the last two columns the luminosity and the effective temperature of the blue tip i.e. the hottest point reached by the model along the blue loop.

Data listed in Tables 1-4 allow us to estimate the dependence of the central H-burning lifetime on the initial He abundance. Oddly enough, this variation is larger for less massive models -16 ÷ 17%-, attains a minimum at $\sim 8.0M_{\odot}$ and then start to increase at higher masses. This behavior is connected with the size of the convective core at the beginning of the central H-burning phase. Note that an increase in the He abundance causes a decrease in the size of the H exhausted region (M_{He}^H), at the ignition of the 3α reaction. This effect is mainly due to the strong dependence of the mean molecular weight on the He abundance which causes an increase in the temperature of the stellar core.

We also find that both the effective temperature and the luminosity of the blue tip at solar metallicity agree quite well with the results obtained by SC93 for $Y=0.28$ and $Z=0.02$. In fact, the difference between our predictions for 7 and 10 M_{\odot} interpolated

linearly at $Y=0.28$ and SC93 results (see their Table 3) is equal or smaller than 0.03 dex. This marginal difference could be due to the different set of molecular opacities adopted by SC93. Even though the formation of the blue loops still presents a non negligible sensitivity to input physics and to the physical assumptions adopted for constructing evolutionary models, this agreement suggests that in this mass range both temperature and luminosity excursions are quite robust predictions.

3.1. The mass-luminosity-effective temperature relation for H-burning stars

To address several astrophysical problems concerning early type stars we need reliable analytical relations connecting luminosity, effective temperature, and stellar mass. This relation is quite useful for β Cephei stars, since it allows us to constrain the luminosity at which these stars cross the β Cephei instability strip and also for comparing the mass estimates based on both evolutionary and pulsational models. A semi-empirical calibration of the mass-luminosity-effective temperature (MLT) relation for early-type stars at solar metallicity was provided by Balona (1984). This calibration was based on the stellar models available at that time (Becker 1981; Maeder 1981), while the zero point was fixed according to empirical mass determinations (Habets & Heintze 1981) and to the absolute magnitude calibration provided by Balona & Shobbrook (1984).

To compare our theoretical predictions for intermediate-mass stars with Balona's empirical calibration, we evaluate the MLT relation for stellar structures with $0.01 \leq Z \leq 0.04$. The relations are derived over the entire mass range and for two different evolutionary phases, namely the ZAMS and the reddest point along the evolutionary track before the overall contraction (OC) phase. The analytical relations we obtain and the uncertainties on the coefficients are listed in Table 5. Interestingly enough, we find that the stellar masses obtained by adopting the Balona's semi-empirical calibration

are only $\approx 7\%$ higher than the stellar masses provided by our relation at solar metallicity. Although our solar metallicity models are on average ≈ 0.15 dex fainter and ≈ 0.02 dex cooler than the Becker's models, the zero point adopted by Balona is supported, within the errors, by the two sets of stellar models.

3.2. He-burning evolutionary phases and the blue loops

A detailed analysis of the dependence of the blue loop on the input physics and physical assumptions for intermediate-mass stars were thoroughly discussed in a seminal paper by Iben (1972) and more recently by Bertelli, Bressan, & Chiosi (1985), Brunish & Becker (1990), Stothers & Chin (1991), and SC93. In the following we outline the main outcomes of present models. Figures 1, 2, and 3 show the evolutionary tracks in the HR diagram for the selected metallicities $Z=0.004$, 0.01 , and $Z=0.02$, and the labeled initial He contents. Data plotted in these figures clearly show that an increase in the He causes a larger excursion toward higher effective temperatures. This suggests that the color width between evolved blue and red stars could be adopted as a He indicator. This effect is due to the fact that an increase in the He content causes a decrease in the mean opacity and an increase in the mean molecular weight of the envelope (Vemury & Stothers 1978), and in turn higher luminosities, hotter effective temperatures, and shorter H and He lifetimes. However, this behavior is not linear with metallicity, and indeed for $Z=0.01$ the blue loop presents a negligible dependence on He content when moving from $Y=0.23$ to $Y=0.27$ (see Figure 2). A quantitative explanation of this effect was not found, however the physical input parameters which trigger and govern the occurrence of the blue loops are manifold (SC93) and beyond the aim of this investigation.

The top panel of Figure 1 shows, as expected, that an increase in the stellar mass widens the temperature excursion of the blue loop. The only exception to this behavior

is the model at $5M_{\odot}$ which shows a smaller blue loop when compared with the model at $4.5M_{\odot}$. This feature was already noted by CCS and they suggested that it is caused by the fact that only the stars with $M \leq 4.5M_{\odot}$ undergo a more efficient first dredge up during the RGB evolution. This occurrence causes an increase in the He content of the envelope, and in turn a decrease in the envelope opacity. As a consequence, even though the He core mass of the $4.5M_{\odot}$ model is smaller than for the $5M_{\odot}$, the blue loop of the former model is larger. The same outcome applies for models at $Z=0.01$ -see top panel of Figure 2-, but the stellar mass who marks the models which experience a sizable first dredge up moves at $M/M_{\odot} \approx 5.5 \div 6.0$ and $M/M_{\odot} \approx 6.0$ for $Y=0.255$ and $Y=0.27$ respectively. Data plotted in Figures 3 and 4 do not show this feature. A detailed check of H-shell burning phases in metal-rich structures ($Z > 0.01$) suggests that the amount of He dredged up during the sinking of the convective envelope does not show, in contrast with less metal-rich models, a local minimum around $5-6 M_{\odot}$. This evidence suggests that the efficiency of the first dredge up in metal-rich structures $-4 \leq M/M_{\odot} \leq 8-$ is mainly governed by opacity and mean molecular weight.

Figure 4 shows the evolution in the HR diagram of SMR models for three different initial He abundances (see labeled values). As expected, these tracks show that the excursion of the blue loop are substantially smaller than in more metal-poor stars. For initial He abundances of $Y=0.29$ and $Y=0.34$, only models with stellar masses ranging from 7.0 to $12.0 M_{\odot}$ show a blue loop which crosses the instability strip. This mass range is further reduced to $7 \div 10M_{\odot}$ for models at $Y=0.37$. In order to address in more detail the effect of the initial He abundance on SMR structures, Figure 5 shows the behavior in the HR diagram of three models at $5, 7$ and $9M_{\odot}$, constructed by adopting the same metal content $-Z=0.04-$ and three different initial He abundances. Data plotted in this figure show that an increase in the He abundance of 10% (≈ 0.03) causes a systematic increase in $\Delta \log L$ of approximately 0.1 dex both during H and He-burning phases. An increase in the

He content from $Y=0.29$ to 0.37 causes, in contrast with more metal-poor stars, a decrease in the temperature excursion of the blue loop. The extension of the loop is also connected with the balance between the envelope thermal time scale (i.e. the Kelvin-Helmoltz time scale) and the nuclear time scale of the internal structure. Therefore, the decrease in the temperature excursion could be due to the decrease in the He-burning lifetime, since the increase in the He content causes an increase in He core mass, and in turn a decrease in τ_{He} . On the basis of this evidence, intermediate-mass stars with $Z > 0.02$ present a much lower probability to produce Cepheid variables. In fact, SMR structures either do not perform the blue loop ($M < 7M_{\odot}$) or spend a short amount of time inside the instability strip ($M \geq 9M_{\odot}$).

Figure 6 shows the change of the central temperature as a function of the central density for selected stellar models. Note that the increase in the initial He abundance from $Y=0.29$ to $Y=0.37$ significantly affects the luminosity of the models, whereas the central properties of the stellar models are only marginally affected at least up to the central He exhaustion. The origin of this behavior can be understood in terms of the quite strong dependence of the H-burning luminosity on the mean molecular weight which presents a substantial increase at higher He contents. Data plotted in this figure show that the thermal properties of intermediate-mass stars present, toward the end of the central He-burning phase, a strong dependence on the initial He content. This effect can have a crucial impact on the final fate of these structures, since they can be forced either to develop a CO core under conditions of moderate or strong electron degeneracy, or to burn carbon (see §3.4).

3.3. Dependence on mass loss and on $^{12}C(\alpha, \gamma)^{16}O$ nuclear reaction rate

To estimate how the mass loss affects the appearance of the blue loop, we computed some additional models by taking into account different mass loss rates available in the

literature. Figure 7 shows the evolutionary tracks for the $8.0M_{\odot}$, $Y=0.37$, $Z=0.04$ model computed by adopting the mass loss parametrizations suggested by Nieuwenhuijzen & de Jager (1990) and by Reimers (1975) respectively. To mimic the effects of a strong mass loss rate, the Reimers' relation was adopted with a large value of the free parameter η , i.e. $\eta = 3$. Note that the typical value for low-mass, metal-poor stars ranges approximately from $\eta = 0.3$ to $\eta = 0.5$. The comparison between evolutionary tracks which include or neglect the mass loss shows quite clearly that the mass loss supplied by the Nieuwenhuijzen & de Jager (1990) relation slightly reduces both the excursion toward higher effective temperatures and the luminosity tickness of the blue loop. This finding confirms previous results for more metal-poor structures by Chin & Stothers (1991) and Salasnich et al. (1999). On the other hand, the evolutionary track constructed by adopting the Reimers relation does not show at all the blue loop. Therefore an efficient mass loss could reduce or inhibit, as originally suggested by Lauterborn, Refsdal, & Roth (1971) and by Lauterborn, & Siquig (1974), the excursion toward the blue, and thus it cannot force metal-rich, intermediate-mass stars inside the instability strip.

Figures 5 and 7 shows the occurrence of small secondary loops during the redward excursion of the blue loop. This feature is due to small increases in the size of the convective core which, in turn, causes small variations in the efficiency of both H-shell and central He-burning. This phenomenon occurs when the core He abundance is lower than $Y_c \approx 0.3$ and it is the analog of the breathing pulses which take place in low-mass stars. The "canonical" breathing pulses become a common feature of central He-burning evolutionary phases when the central He abundance is lower than ≈ 0.1 . However, their appearance is presently inhibited in our evolutionary code. On the contrary, the phenomenon described above takes place at earlier evolutionary phases and was not artificially quenched. This notwithstanding some models constructed by inhibiting the appearance of such a phenomenon present only negligible differences in both central and He-shell burning lifetimes.

As already mentioned in §1, the $^{12}\text{C}(\alpha, \gamma)^{16}\text{O}$ nuclear reaction rate is a key physical ingredient in the evolutionary behavior of intermediate-mass stars. In fact, the M_{CO} at the He exhaustion and the C/O ratio inside this core strongly depends on this reaction rate. Even though a thorough analysis of its effects is beyond the aim of this investigation, we are interested in testing the dependence of our results on the adopted reaction rate. To account for this effect we construct selected models by adopting the $^{12}\text{C}(\alpha, \gamma)^{16}\text{O}$ reaction rate provided by CF88. It is worth mentioning that for temperatures typical of He-core burning phase, i.e. $T \approx 3 \times 10^8$ K, the reaction rate provided by CFHZ85 is approximately 2.35 larger than the CF88 one. Even though this reaction rate is still affected by a large uncertainty (CF88; Buchmann 1997), recent theoretical constraints based on evolution and nucleosynthesis in SNe type II progenitors support a $^{12}\text{C}(\alpha, \gamma)^{16}\text{O}$ reaction rate larger than suggested by CF88 (Woosley & Weaver 1995; Hoffman et al. 1999). This is the reason why in our investigation the evolutionary models are constructed by adopting the reaction rate provided by CFHZ85. To account for current uncertainties, we perform several numerical experiments by increasing the CF88 reaction rate by 1.7. This enhancement factor, which corresponds at 300 Kev to an S -factor of 170 Kev barns, accounts also for solar abundance distribution (Weaver & Woosley 1993), but see also Nomoto & Hashimoto (1988), and Umeda et al. (1999) for different assumptions.

Figure 8 shows the location in the H-R diagram of selected stellar models at solar chemical composition constructed by adopting different values of the $^{12}\text{C}(\alpha, \gamma)^{16}\text{O}$ rate. Note that the use of different rates does not change, in this mass range, the excursion of the blue loop. This finding supports the results of previous investigations (Chin & Stothers 1991). At the same time, we are also interested in testing the dependence of the central He-burning lifetime (τ_{He}), of the CO core mass and C/O ratio at the He exhaustion, on this parameter. We find that for models at 5, 7, and 10 M_{\odot} the τ_{He} values based on the CFHZ85 rate are $\approx 9, 7,$ and 8% longer than the τ_{He} values based on the CF88 rate (see

Table 6), while the CO core mass at the He exhaustions in the former models are on average 3% larger. Therefore, the numerical experiments we performed seem to suggest that current uncertainties on the $^{12}\text{C}(\alpha, \gamma)^{16}\text{O}$ reaction rate marginally affect the Cepheid evolutionary properties. This evidence is further supported by the fact that both the time spent inside the instability strip and the tip of the blue loop are marginally affected by this input parameter. However, note that the total crossing time for the $5 M_{\odot}$ model based on the CF88 rate is approximately 25% shorter than the model based on the CFHZ85 rate. Further theoretical studies are necessary to investigate the impact of this behavior on short-period Cepheids.

Obviously the C/O abundance ratio is, significantly affected by this nuclear reaction rate, and indeed models based on the CFHZ85 rate present a decrease of a factor of 3 when compared with the models based on the CF88 rate. Data listed in Table 6 also show that this effect does not depend on the stellar mass. Note that the C/O ratio affects the lifetime of white dwarfs (WD), since along the cooling sequence the gravothermal energy strongly depends on the chemical profile of the inner layers. Therefore, we can also expect that the $^{12}\text{C}(\alpha, \gamma)^{16}\text{O}$ reaction rate affects the evolutionary properties along the WD cooling sequence.

3.4. Dependence of M^{up} on metallicity

We now discuss the evolutionary behavior of metal-rich structures after the central He exhaustion. At the end of the central He-burning the ultimate fate of a star depends on its total mass. Stellar structures more massive than a critical value -the so-called M_{up} - quietly ignite carbon, evolve toward the subsequent evolutionary phases and eventually end up their evolution as core collapse supernovae. Stellar structures less massive than M_{up} undergo a full electronic degeneracy inside the CO core during the AGB phase. These stars

end up with a carbon deflagration -thermonuclear supernovae-, if and when the mass loss allows the CO core to become larger than the Chandrasekhar mass $M_{Ch} \approx 1.4M_{\odot}$. The dependence of M^{up} on the initial chemical composition has already been discussed by a number of authors (Becker 1981; Tornambè & Chieffi 1986, hereinafter TC; Castellani et al. 1990; Cassisi & Castellani 1993). However, these investigations were focused on structures with $Z \leq 0.02$ and only recently extended to higher metallicities by Umeda et al. (1999).

By adopting the procedure suggested by TC, we find that the upper mass limit for carbon deflagration in SMR stars are $M^{up} = 9.5 \pm 0.5M_{\odot}$, $8.7 \pm 0.2M_{\odot}$, and $7.7 \pm 0.2M_{\odot}$ for $Y=0.29$, 0.34 and $Y=0.37$, respectively, while at solar chemical composition it is $M^{up} = 7.7 \pm 0.5M_{\odot}$. Figure 9 shows the comparison between different estimates of M^{up} values as a function of metallicity. The solid line refers to M^{up} values of models constructed by adopting $Y=0.23$ for $Z < 0.01$, $Y=0.255$ for $Z=0.01$, $Y=0.289$ for $Z=0.02$, and $Y=0.34$ for $Z=0.04$. Our estimates have been implemented with the M^{up} values for $Z=10^{-10}$ and 10^{-6} provided by Cassisi & Castellani (1993).

Data plotted in this figure show that for metallicities $Z \geq 0.01$ our estimates agree quite well with the M^{up} values estimated by Umeda et al. (1999). This notwithstanding their M^{up} value for $Z=0.001$ is approximately $1M_{\odot}$ larger than our value. No clear explanation for this discrepancy was found, since the models constructed by these authors rely on update input physics. At the same time, they adopt a higher initial He content ($Y=0.249$ versus $Y=0.23$), and therefore their M^{up} value should be smaller than our estimate. On the other hand, our M^{up} values are systematically larger than the estimates provided by TC. However, predictions provided by TC are based on evolutionary models in which the "canonical" breathing pulses at the end of central He-burning were not inhibited. The difference between TC and our M^{up} values confirms the results by Caputo et al. (1989), and indeed they found that the inclusion of breathing pulses, regardless of the stellar metallicity,

causes an increase in the mass of CO core, and in turn a decrease in M^{up} of $\approx 0.5M_{\odot}$.

Finally, we note the strong dependence of M^{up} on the initial He abundance, and indeed an increase in the He content from 0.34 to 0.37 causes a decrease in the M^{up} value of the order of one solar mass. This effect is due to the increase in the size of the convective core during the central H-burning phase which, in turn causes an increase in the size of the CO core at the end of the central He-burning phase.

4. The mass-luminosity relation of classical Cepheids

The accuracy of distance determinations based on the Period-Luminosity (PL) and on the Period-Luminosity-Color (PLC) relations of classical Cepheids is widely discussed in the current literature. The key point in this lively debate is to assess whether Cepheids obey to universal PL and PLC relations or their pulsation behavior depends on chemical composition. Several empirical and theoretical facts such as the mean radius, color and the pulsation amplitudes strongly support the evidence that the Cepheid properties do depend on metallicity (Gascoigne 1974; Bono Caputo, & Marconi 1998; Paczyński & Pindor 2000). Moreover, current nonlinear, convective pulsation models suggest, at variance with some empirical evidence, that metal-rich Cepheids are fainter than metal-poor ones.

This finding relies on the adopted pulsation framework (linear vs. nonlinear, coupling between pulsation and convection) and on the ML relation adopted for constructing pulsation models. The dependence of the ML relation on chemical composition has been discussed in several papers (Chiosi, Wood, & Capitanio 1993, hereinafter CWC; Saio & Gautschy 1998; ABHA; Bono et al. 1999a; Bono et al. 2000). However, the ML relations derived by these authors rely on old input physics (CWC; Bono et al. 1999a) or assume at fixed stellar mass a mean luminosity level (Bono et al. 1999a,b; ABHA). To estimate the

time spent inside the instability strip, we selected both H (1st crossing) and He-burning (2nd and 3rd crossing) phases located between the fundamental blue and red edges for $M > M^*$, and between the first overtone blue edge and the fundamental red edge for $M < M^*$, where M^* is the predicted upper mass limit for the occurrence of first overtone pulsators. This limit is $7M_{\odot}$ for $Z=0.004$, 0.01 and $5M_{\odot}$ for $Z=0.02$. Note that for models at $Z=0.01$ we adopted the instability edges constructed by adopting $Y=0.25$ and $Z=0.008$. The time spent inside the instability strip during the approach to the main sequence and after the AGB phase ($M \leq M^{up}$) are substantially shorter than the crossings during H and He burning phase and have been neglected.

Due to the fine mass resolution adopted for constructing the different sets of evolutionary models, we also investigated the minimum and the maximum mass which perform a blue loop and crosses the red edge of the instability strip. Table 7 lists these mass values for the different chemical compositions. We confirm the dependence of the minimum mass on metallicity suggested by ABHA, and indeed we find that for $\Delta Y/\Delta Z=2.5$ the M_{min} changes from $\approx 3.25M_{\odot}$ at $Z=0.004$ to $\approx 4.25M_{\odot}$ at $Z=0.01$, and to $\approx 4.75M_{\odot}$ at $Z=0.02$. Even though ABHA adopted slightly different He contents our minimum masses are quite similar to the values they predicted. It is worth noting that M_{min} presents a similar dependence on He content, since an increase in He moves M_{min} toward higher values. We also find that our upper mass limits for structures which perform the blue loop are for $Z=0.004$ and $Z=0.02$ roughly $1 M_{\odot}$ larger than predicted by ABHA. A firm explanation for this discrepancy was not found, since the two sets of evolutionary predictions were constructed by adopting the same opacity tables and the same convective instability criterion. However, this difference is not surprising, since as demonstrated by Chin & Stothers (1991) the appearance of the blue loop is also affected by marginal changes in input parameters.

Once the evolutionary phases which produce Cepheids are selected, we estimate the time spent inside the instability strip during the three subsequent crossings. Figure 11 shows the ratio between the three crossing times and the total time spent inside the instability strip as a function of stellar mass. Data plotted in this figure show quite clearly that the time ratios present a strong dependence on metallicity. In fact, the time ratios of metal-poor structures suggest that in the mass range $4 \div 6M_{\odot}$ stellar structures spend more than 80% of their Cepheid lifetime along the 2nd crossing (t^{II} , triangles), while they spend less than 20% along the 3rd one (t^{III} squares) and a negligible amount of time along the 1st (t^I , circles). On the other hand, more massive structures ($M/M_{\odot} \geq 7$) present a different behavior, with $t^{II} \approx t^{III}$ for $M/M_{\odot} = 7$, while for higher masses the time spent during the 3rd crossing (H and He-shell burning) becomes longer than the 2nd one (central He and H-shell burning). At the same time, the duration of the 1st crossing (H-shell burning) increases and becomes of the order of 15 – 20% for $M/M_{\odot} = 10-11$ stellar structures. This suggests that for $M/M_{\odot} = 9$ the probability to detect a Cepheid during its redward excursion (1st + 3rd crossing) is almost a factor of 2 larger than during its blueward excursion (2nd crossing). At the same time, data plotted in the top panel suggest that when moving from low to high-mass Cepheids the probability to detect a Cepheid during the 1st crossing increases by more than one order of magnitude.

The time ratios of stellar structures at $Z=0.01$ present a different behavior when moving from low to high-mass Cepheids. In fact, t^{II} is generally longer than t^{III} with the exception of the model at $M = 5M_{\odot}$. Oddly enough, the time ratios of solar metallicity models present an opposite behavior when compared with metal-poor structures. In fact in the low-mass range the time spent during the 3rd crossing is longer than in the 2nd one. The two ratios become identical for $M/M_{\odot} = 7$, attain similar values up to $M/M_{\odot} = 10$, but for higher masses t^{II} is substantially longer than t^{III} . These findings suggest that in the mass range $7 \leq M/M_{\odot} \leq 10$ the probability to detect a LMC Cepheid during its blueward

excursion is much higher than for SMC and Galactic Cepheids. At the same time they also suggest that the probability to detect short-period Galactic and Magellanic Cepheids during the 1st crossing is quite negligible.

The previous findings do not confirm the old rule of thumb that classical Cepheids are mainly evolving from the red to the blue (2nd crossing). In fact we find that the time spent during the subsequent crossings does depend not only on the metallicity but also on the stellar mass. We also tested the dependence of the three crossing times on the He content, and we found that it is vanishing for stellar structures at $Z=0.01$ and $Z=0.02$ and smaller than 10% for $Z=0.004$. On the basis of these results and to avoid misleading effects in the selection of the mean luminosity, we decided to derive the ML relation by including for each mass all the evolutionary points located inside the instability strip. Moreover, to properly account for the time spent during the three subsequent crossings, the individual points were weighted according to the individual evolutionary times. Thanks to the large range of both metallicities and He contents covered by our models the analytical ML relation was estimated by including the dependence on chemical composition. As a result we obtain:

$$\begin{aligned} \log L = & 0.90 & +3.35 \log M & +1.36 \log Y & -0.34 \log Z & \sigma=0.02 \\ & \pm 0.02 & \pm 0.03 & \pm 0.13 & \pm 0.02 \end{aligned}$$

where σ is the standard deviation and the other symbols have their usual meaning. Interestingly enough we find that this ML relation is in very good agreement with the relation adopted by Bono et al. (1999a) and by ABHA. In fact, at solar composition the discrepancy with these relations depends on the mass value but it is always smaller than $\Delta \log L = 0.1$. This confirms that the luminosity of intermediate-mass stars predicted by canonical evolutionary models is, within current uncertainties, well-constrained.

Finally, we mention that the fundamental periods⁷ at the center of the instability

⁷In the region of the instability strip in which only the first overtone is unstable the

strip provide a plain support to the empirical evidence that the period distribution of Magellanic Cepheids presents a sharp break in the short-period tail (Alcock et al. 1999; Udalski et al. 1999a,b). In fact, the OGLE samples clearly show that the fundamentalized period distribution of LMC Cepheids presents a sharp break at $\log P \approx 0.4$, while in SMC Cepheids such a break is located at $\log P \approx 0.1$. Predicted minimum fundamental periods for $Z=0.004$ and $Z=0.01$ attain quite similar values. In fact, during the 2nd and the 3rd crossing they range from $\log P \approx 0.08$ to 0.18 for $Z=0.004$ and from $\log P \approx 0.34$ to $\log P \approx 0.44$ for $Z=0.01$.

5. Summary and Conclusions

We investigated the evolutionary properties of metal-rich ($Z=0.01$ and 0.02) and SMR ($Z=0.04$) intermediate-mass stars ($3 \leq M/M_{\odot} \leq 15$). These evolutionary calculations together with similar predictions for low-mass stellar structures presented in previous investigations (Bono et al. 1997a,b,c) supply a homogeneous theoretical framework for metal-rich and SMR stellar populations. To account for the evolutionary behavior of stellar systems in the MCs this theoretical scenario was implemented with two sets of models constructed by adopting $Z=0.004$ and $Z=0.01$ respectively. Owing to current empirical and theoretical uncertainties on the He to metal enrichment ratio and to the strong dependence of stellar structures on He content the evolutionary calculations were performed by adopting at least two different He abundances. The evolutionary tracks were computed from the ZAMS up to the central He exhaustion and often up to the phases which precede the carbon ignition or to the beginning of the thermal pulse phase.

pulsation period was fundamentalized i.e. the first overtone period was transformed into a fundamental period by adopting $\log P_F = \log P_{FO} + 0.127$.

We derived the mass-luminosity-effective temperature relations for intermediate-mass stars along the ZAMS and during the overall contraction phase and we find that at solar chemical composition the stellar masses predicted by the new relations are in good agreement with values given by the semi-empirical calibration suggested by Balona (1984). Current models support the evidence that the M^{up} value, i.e. the cut-off mass between stars that ignite carbon under nondegenerate conditions and stars that form a strong degenerate CO core, strongly depends on the metallicity. This finding confirms the results by Cassisi & Castellani (1993) and by Umeda et al. (1999). It is worth noting that toward higher metallicities $-Z > 0.02-$ the M^{up} value increases and at $Z=0.04$ becomes approximately equal to $8 M_{\odot}$, the exact value strongly depends on the adopted initial He content. This result is quite interesting since it could have a substantial impact on chemical evolution models and on the luminosity function of white dwarfs in SMR stellar systems.

Thanks to the wide range of chemical compositions covered by current evolutionary calculations it has been possible to investigate in detail the evolutionary properties of classical Cepheids. We find that the probability to detect long-period Cepheids in SMR stellar systems is substantially smaller than in more metal-poor systems. This effect is due to the fact that the range of stellar masses which perform the blue loop narrows when moving toward metal-rich and SMR structures and also because the evolutionary time spent inside the instability strip is shorter than for more metal-poor ones.

We find that the Cepheid crossing times also depends on the stellar mass. As a matter of fact, low-mass, metal-poor Cepheids spend a substantial portion of their lifetime along the 2nd crossing, while at higher masses ($M/M_{\odot} \geq 8$) the 3rd crossing time becomes longer than the 2nd one. On the contrary, models at solar chemical composition present an opposite behavior i.e. the 3rd crossing time is longer than the 2nd one among low-mass Cepheids, whereas it becomes shorter among high-mass Cepheids. At the same time, we

also find that the crossing times present a nonlinear dependence on metallicity, and indeed for models at $Z=0.01$ the 3rd crossing time is longer than the 2nd one over the entire mass range. It is worth mentioning that the 1st crossing time is generally negligible with the exception of high-mass, metal-poor stars for which it becomes of the order of 15-20% of the total crossing time.

Finally we mention that the outcomes concerning the difference in the crossing times could be directly tested on empirical data. In fact, these results seem to suggest that at fixed period the spread in luminosity among SMC Cepheids should be larger than among LMC Cepheids. This result might partially account for the empirical evidence, originally pointed out by Caldwell & Coulson (1986) in optical bands and by Laney & Stobie (1986) in NIR bands, that the apparent dispersions of both PL and PLC relations are systematically larger for SMC than for LMC Cepheids. However, a firm constraint on this effect cannot be provided, since the LMC presents a negligible tickness along the line-of-sight, whereas we see the the SMC almost end-on. Therefore the luminosity scatter is expected, due to depth effects, to be larger among SMC than LMC Cepheids. Note that the increase at lower metal contents in the intrinsic dispersion of PL and PLC relations has a marginal effect on distance determinations. In fact, according to Bono et al. (1999b) a systematic shift in the luminosity level marginally affects the slope of these relations, once the metallicity dependence has been properly taken into account.

At the same time, these findings suggest that the period changes caused by evolutionary effects should depend not only on the pulsation period but also on the chemical composition. Current empirical estimates seem to suggest that period changes among SMC Cepheids present a different behavior when compared with LMC Cepheids (Deasy & Wayman 1985). Unfortunately we lack a quantitative estimate of this effect, and in particular of its dependence, if any, on the period. In the near future, photometric data collected by large

scale surveys can supply the accuracy needed to shed new light on these still unsettled questions and to constrain both evolutionary and pulsational predictions.

We wish to thank V. Castellani for valuable suggestions and for a critical reading of an early draft of this manuscript. One of us (S.C.) warmly acknowledges for the hospitality at the MPA Institute (Garching) during which part of this paper was written. We acknowledge an anonymous referee for his/her pertinent comments and useful suggestions that improved the content and the readability of the paper. The sets of evolutionary models discussed in this investigation can be retrieved from the WWW site <http://gipsy.cjb.net>, while the isochrones are available upon request to the authors. This research has made use of NASA's Astrophysics Data System Abstract Service and of SIMBAD database operated at CDS, Strasbourg, France. This work was supported by MURST -Cofin98- under the scientific project: "Stellar Evolution". Partial support by ASI and CNAA is also acknowledged.

REFERENCES

- Alcock, C., & Paczynski, B. 1978, *ApJ*, 223, 244
- Alcock, C., et al. 1999, *AJ*, 117, 920
- Alexander, D. R., & Ferguson, J. W. 1994, *ApJ*, 437, 879
- Alibert, Y., Baraffe, I., Hauschildt, P., & Allard, F. 1999, *A&A*, 344, 551 (ABHA)
- Balona, L. A. 1984, *MNRAS*, 211, 973
- Balona, L. A. 1994, *MNRAS*, 267, 1060
- Balona, L. A., Dziembowski, W. A., & Pamyatnykh, A. 1997, *MNRAS*, 289, 25
- Balona, L. A., & Laney, C. D. 1995, *MNRAS*, 276, 627
- Balona, L. A., & Shobbrook, R. R. 1984, *MNRAS*, 211, 375
- Becker, S. A. 1981, *ApJS*, 45, 475
- Becker, S. A., & Iben, I. Jr. 1981, *ApJ*, 237, 111
- Bertelli, G., Bressan, A., & Chiosi, C. 1985, *A&A*, 150, 33
- Bertelli, G., Bressan, A., Chiosi, C., & Ng, Y. K. 1996, *A&A*, 310, 115
- Bono, G., Caputo, F., Cassisi, S., Castellani, V., & Marconi, M. 1997a, *ApJ*, 479, 279
- Bono, G., Caputo, F., Cassisi, S., Castellani, V., & Marconi, M. 1997c, *ApJ*, 489, 822
- Bono, G., Caputo, F., Cassisi, S., Incerpi, R., & Marconi, M. 1997b, *ApJ*, 483, 811
- Bono, G., Caputo, F., Castellani, V., & Marconi, M. 1999b, *ApJ*, 512, 711
- Bono, G., Caputo, F., & Marconi, M. 1998, *ApJ*, 497, L43

- Bono, G., Castellani, V., & Marconi, M. 2000, *ApJ*, 529, 293
- Bono, G., Marconi, M., & Stellingwerf, R. F. 1999a, *ApJS*, 122, 167
- Bressan, A., Chiosi, C., & Fagotto, F. 1994, *ApJS*, 94, 63
- Bressan, A., Fagotto, F., Bertelli, G., & Chiosi, C. 1993, *A&AS*, 100, 647
- Brocato, E., & Castellani, V. 1993, *ApJ*, 410, 99
- Brunish, W. M., & Becker, S. A. 1990, *ApJ*, 351, 258
- Buchmann, L. 1997, *ApJ*, 479, 153
- Caldwell, J.A.R., & Coulson, I.M. 1986, *MNRAS*, 218, 223
- Canuto, V. M. 2000, *ApJ*, 534, L113
- Caputo, F., Chieffi, A., Tornambé, A., Castellani, V. & Pulone, L. 1989, *ApJ*, 340, 241
- Carigi, L., Colin, P., & Peimbert, M. 1999, *ApJ*, 514, 787
- Cassisi, S., & Castellani, V. 1993, *ApJS*, 88, 509
- Cassisi, S., Castellani, V., Salaris, M., & Straniero, O. 1994, *A&A*, 282, 760
- Cassisi, S., Castellani, V., Degl'Innocenti, S., & Weiss, A. 1998, *A&AS*, 129, 267
- Castellani, V., Chieffi, A., & Straniero, O. 1990, *ApJS*, 74, 463
- Castellani, V., Chieffi, A., & Tornambé, A. 1983, *ApJ*, 272, 249
- Castellani, V., Degl'Innocenti, S., Fiorentini, G., Lissia, M., & Ricci, B. 1999, *Phys. Rep.*, 281, 309
- Castellani, V., Degl'Innocenti, S., & Marconi, M. 1999, *MNRAS*, 303, 265

- Caughlan, G. A., & Fowler, W. A. 1988, *At. Data Nucl. Data Tables*, 40 , 283 (CF88)
- Caughlan, G. A., Fowler, W. A., Harris, M. J., & Zimmerman, B. A., 1985, *At. Data Nucl. Data Tables*, 32, 197 (CFHZ85)
- Chiappini, C., Matteucci, F., & Gratton, R. 1997, *ApJ*, 447, 765
- Chieffi, A., & Straniero, O. 1989, *ApJS*, 71, 47
- Chin, C. W., & Stothers, R. B. 1991, *ApJS*, 77, 299
- Chiosi, C., Bertelli, G., & Bressan, A. 1992, *ARAA*, 30, 235
- Chiosi, C., Bertelli, G., Meylan, G., & Ortolani, S. 1989, *A&A*, 219, 167
- Chiosi, C., & Maeder, A. 1986, *ARAA*, 24, 329
- Chiosi, C., Wood, P. R., & Capitanio, N. 1993, *ApJS*, 86, 541 (CWC)
- Deasy, H. P., & Wayman, P. A. 1985, *MNRAS*, 212, 395
- Esteban, C., Peimbert, M., Torres-Peimbert, S., & Garcia-Rojas, J. 1999, *RevMexAA*, 35, 85
- Gascoigne, S. C. B. 1974, *MNRAS*, 166, 25
- Gieren, W. P., Fouqu e, P., & Gomez, M. 1998, *ApJ*, 496, 17
- Gies, D. R., & Lambert, D. L. 1992, *ApJ*, 387, 673
- Girardi, L., Bressan, A., Bertelli, G., & Chiosi, C. 2000, *A&AS*, 141, 371
- Grevesse, N. 1991, in *IAU Symp. 145, Evolution of Stars: the Photospheric Abundance Connection*, ed. G. Michaud, A. Tutukov (Dordrecht: Kluwer), 63
- Groenewegen, M. A. T., & Oudmaijer, R. D. 2000, *A&A*, accepted, astro-ph/0002325

Habets, G. M. H. J. & Heintze J. R. W. 1981, A&AS, 46, 193

Hoffman, R. D., Woosley, S. E., Weaver, T. A., Rauscher, T., & Thielemann, F. -K. 1999,
ApJ, 521, 735

Iben, I. Jr. 1972, ApJ, 178, 433

Iben, I. Jr., & Livio, M. 1993, PASP, 105, 1373

Iglesias, C. A., & Rogers, F. J. 1996, ApJ, 464, 943

Kennicutt, R. C., et al. 1998, ApJ, 498, 181

Krishna-Swamy, K. S. 1966, ApJ, 145, 174

Laney, C. D., & Stobie, R. S. 1986, MNRAS, 222, 449

Lattanzio, J. C. 1991, ApJS, 76, 215

Lauterborn, D., & Refsdal, S., & Weigert, A. 1971, A&A, 10, 97

Lauterborn, D., & Siquig, R. A. 1974, ApJ, 191, 589

Luck, R. E., Moffett, T. J., Barnes, T. G. III, & Gieren, W. P. 1998, AJ, 115, 605

Maeder, A. 1981, A&A, 102, 401

Maeder, A., & Meynet, G. 1987, A&A, 182, 243

Meynet, G., Maeder, A., Schaller, G., Schaerer, D., & Charbonnel, C. 1994, A&AS, 103, 97

Nieuwenhuijzen, H., & de Jager, C. 1990, A&A, 231, 134

Nomoto, K., & Hashimoto, M., 1988, Phys. Rep., 163, 13

Paczynski, B., & Pindor, B. 2000, ApJ, submitted, astro-ph/0001417

- Pagel, B. E. J., Simonson, E. A., Terlevich, R. J., Edmunds, M. G. 1992, MNRAS, 255, 325
- Pamyatnykh, A. 1999, AcA, 49, 119
- Peimbert, M., & Peimbert, A. 2000, in IAU Symp. 198, in press, astro-ph/0002120
- Peimbert, M., Peimbert, A., & Ruiz, M. T. 2000, ApJ, accepted, astro-ph/0003154
- Reimers, D. 1975, Mém. Soc. Roy. Sci. Liège 6^e Ser., 8, 369
- Renzini, A. 1994, A&A, 285, L5
- Saio, H., & Gautschy, A. 1998, ApJ, 498, 360
- Sakashita, S., & Hayashi, C. 1959, Prog. Theor. Phys., 22, 830
- Salaris, M., Cassisi, S. 1996, A&A, 305, 858 (SC)
- Salaris, M., Dominguez, I., Garcia-Berro, E., Hernanz, M., Isern, J., & Mochkovitch R. 1997, ApJ, 486, 413
- Salasnich, B., Bressan, A., & Chiosi, C. 1999, A&A, 342, 131
- Sasselov, D. D., et al. 1997, A&A, 324, 471
- Schaerer, D., De Koter, A., Schmutz, W. & Maeder, A. 1996, A&A, 312, 475
- Schwarzschild, M., & Härm, R. 1958, ApJ, 128, 348
- Seaton, M. J., Yuan, Y., Mihalas, D. & Pradhan, A. K. 1994, MNRAS, 266, 805
- Stothers, R. B., & Chin, C. W. 1991, ApJ, 381, L67
- Stothers, R. B., & Chin, C. W. 1992, ApJ, 390, 136
- Stothers, R. B., & Chin, C. W. 1993, ApJ, 412, 294 (SC93)

Stothers, R. B., & Chin, C. W. 1994, *ApJ*, 431, 797

Straniero, O. 1988, *A&AS*, 76, 157

Thielemann, F.-K., Nomoto, K., & Hashimoto, M. 1996, *ApJ*, 460, 408

Tornambé, A., & Chieffi, A. 1986, *MNRAS*, 220, 529 (TC)

Udalski, A., et al. 1999a, *AcA*, 49, 223

Udalski, A., et al. 1999b, *AcA*, 49, 437

Umeda, H., Nomoto, K., Yamaoka, H., & Wanajo, S. 1999, *ApJ*, 513, 861

Vemury, S. K. & Stothers, R. 1978, *ApJ*, 225, 939

Waelkens, C., van den Abeele, K., & van Winckel, H. 1991, *A&A*, 251, 69

Weaver, T. A., & Woosley, S. E., 1993, *Phys. Rep.*, 227, 65

Weiss, A., Peletier, R. F., & Matteucci, F. 1995, *A&A*, 296, 73

Woosley, S. E., & Weaver, T. A. 1995, *ApJS*, 101, 181

Zoccali, M., Cassisi, S., Bono, G., Piotto, G., Rich, R. M. & Djorgovski, S. G. 2000, *ApJ*,
accepted, astro-ph/0003004

Fig. 1.— Evolutionary tracks in the HR diagram for stellar models constructed by adopting a fixed metallicity $Z=0.004$ and two different He contents namely $Y=0.23$ (top panel) and $Y=0.27$ (bottom panel). The tracks cover both H and He-burning phases. The stellar masses are labeled.

Fig. 2.— Similar to Figure 1, but for models constructed by adopting $Z=0.01$ and three different He contents: $Y=0.23$ (top panel), 0.255 (middle panel), and 0.27 (bottom panel).

Fig. 3.— Similar to Figure 1, but for solar metallicity models at $Y=0.27$ (top panel), and $Y=0.289$ (bottom panel).

Fig. 4.— Similar to Figure 1, but for SMR models constructed by adopting three different He contents: $Y=0.29$ (top panel), 0.34 (middle panel), and 0.37 (bottom panel).

Fig. 5.— Theoretical HR diagram for selected SMR models constructed by adopting different He contents and stellar masses (see labeled values).

Fig. 6.— Evolution of central physical conditions -temperature vs density- during both H and He burning phases for models constructed by adopting a fixed stellar mass $-M/M_{\odot}=5.0, 7.0, 9.0-$ and three different He abundances (see labeled values).

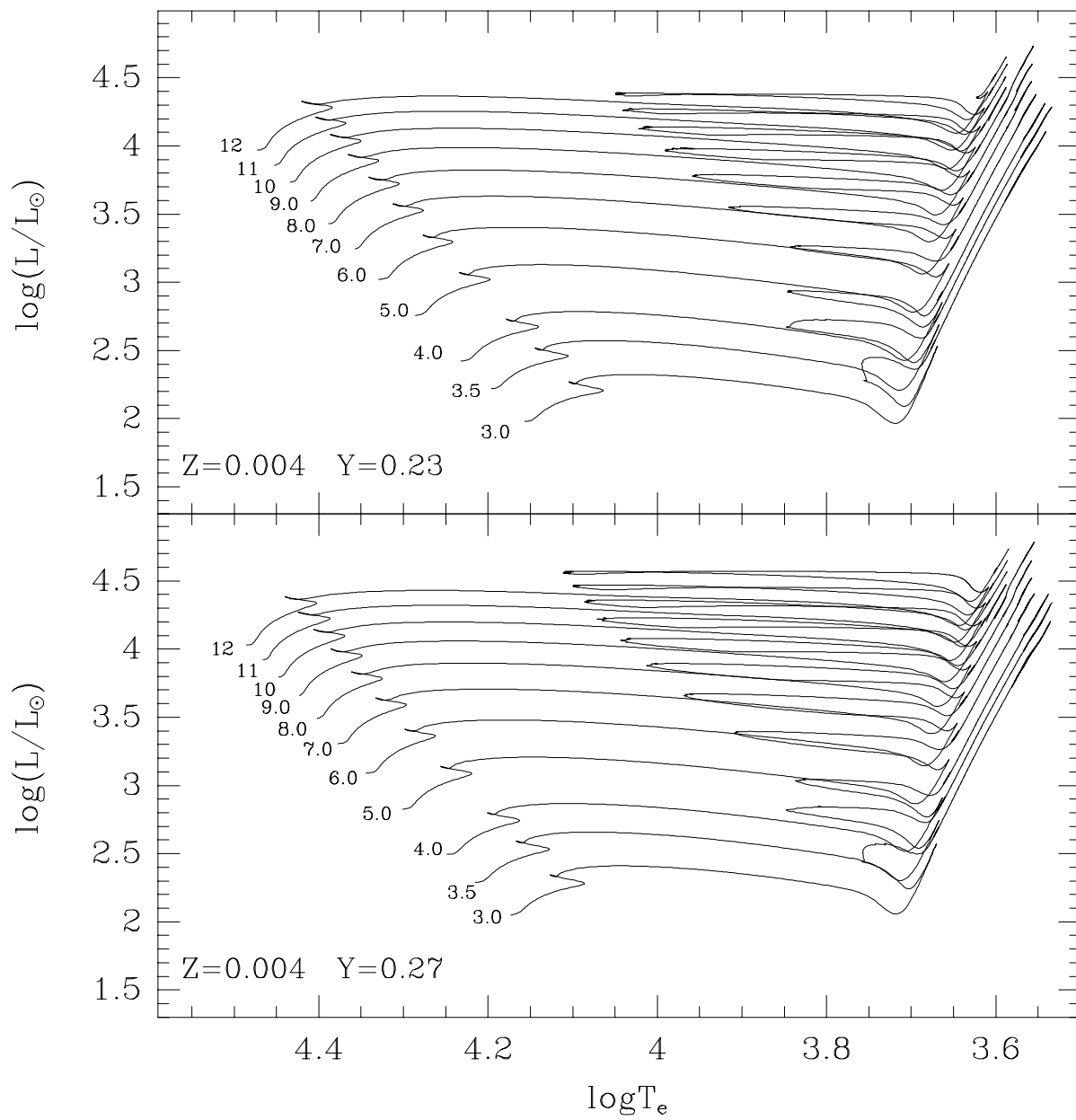
Fig. 7.— Theoretical HR diagram showing a $8.0M_{\odot}$ model $-Z=0.04, Y=0.37-$ computed by adopting different empirical mass loss rates. The solid line refers to the canonical evolutionary track -no mass loss-, while the dashed and the dashed-dotted line to evolutionary tracks which include the mass loss relations provided by Nieuwenhuijzen & de Jager (1990) and by Reimers (1978) respectively. See text for more details.

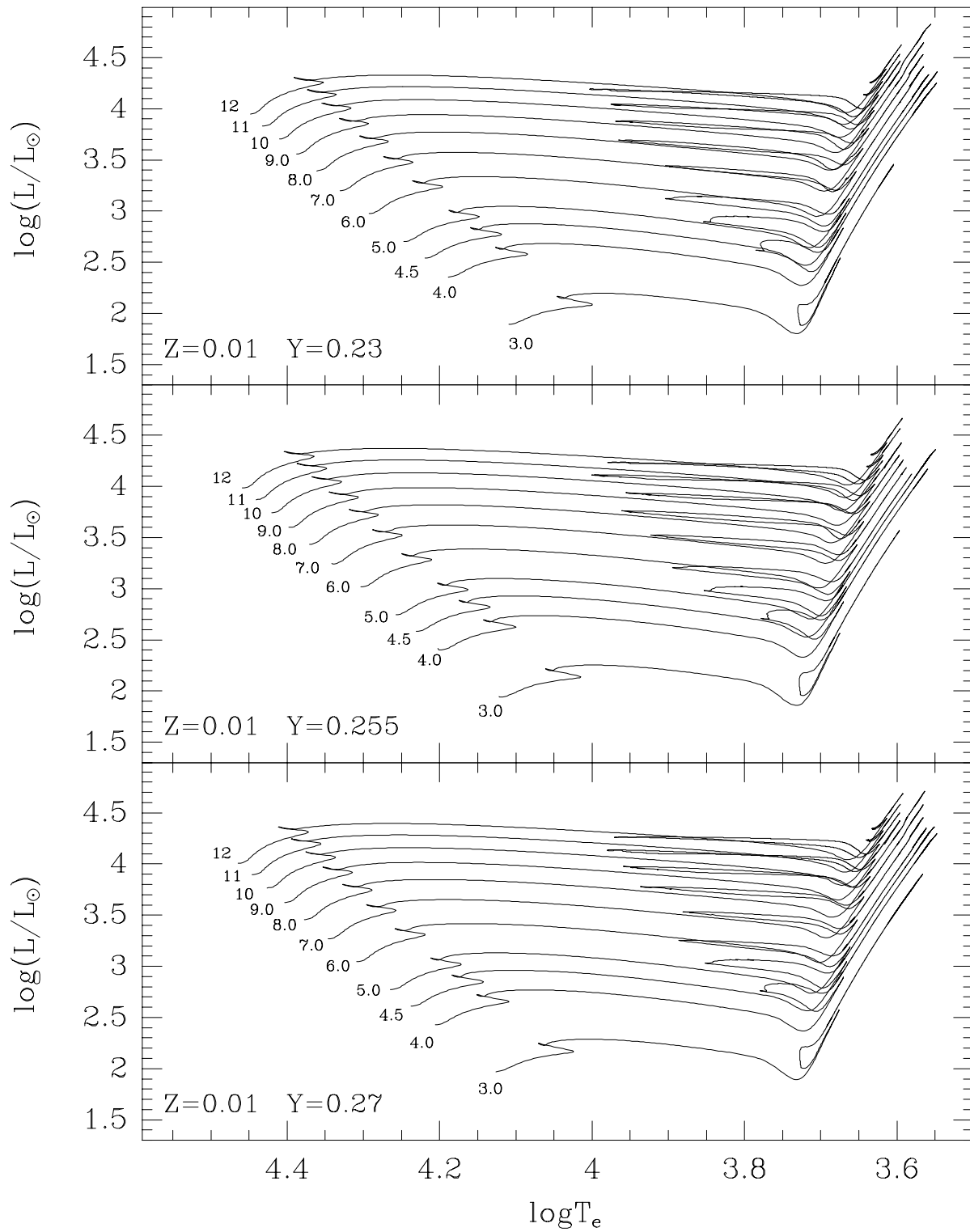
Fig. 8.— Evolution in the HR diagram of stellar structures constructed at fixed chemical composition and stellar mass but different values for the $^{12}C(\alpha, \gamma)^{16}O$ nuclear reaction rate.

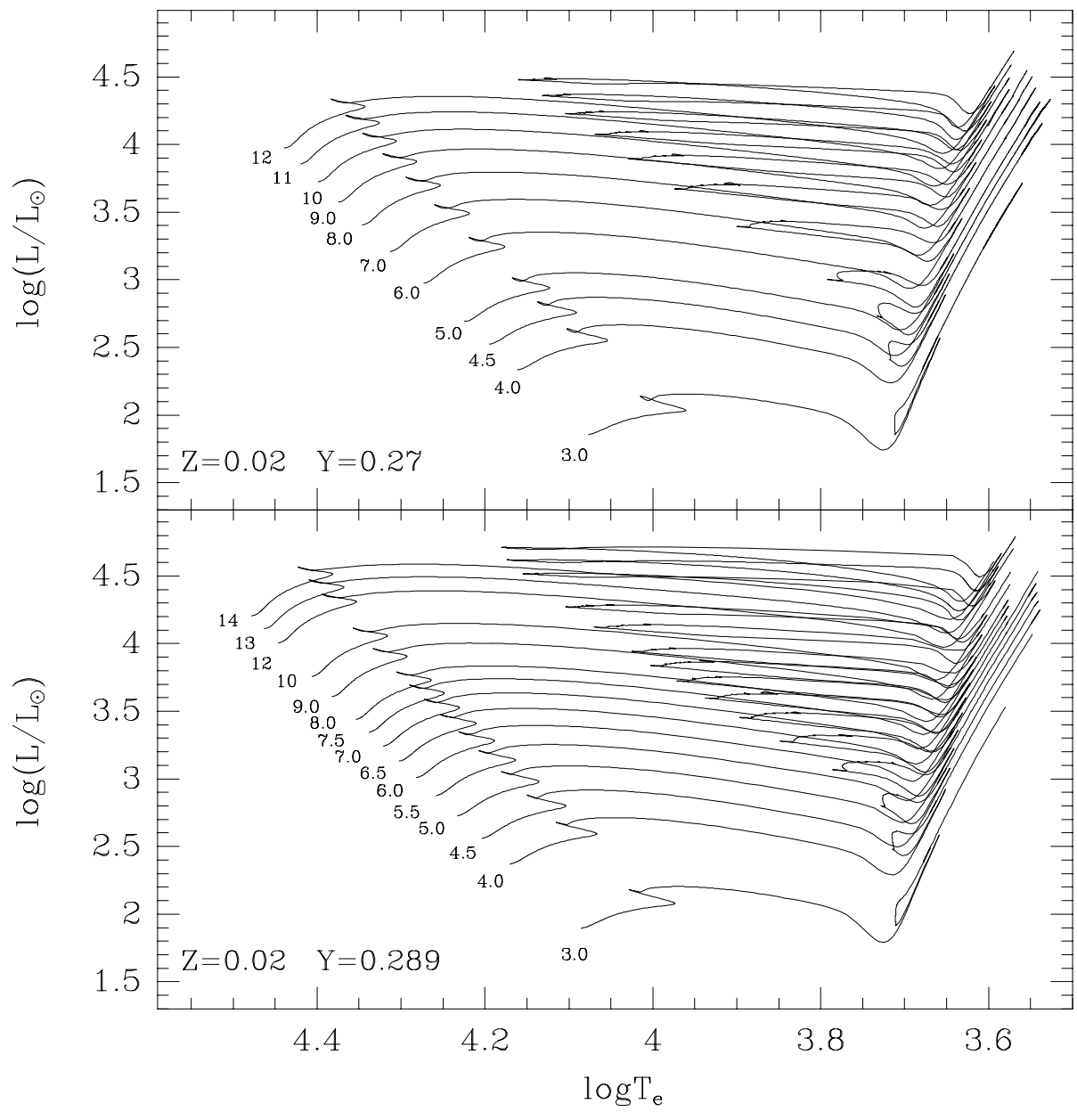
Fig. 9.— The behavior of M^{up} as a function of the logarithmic metallicity. The M^{up} values

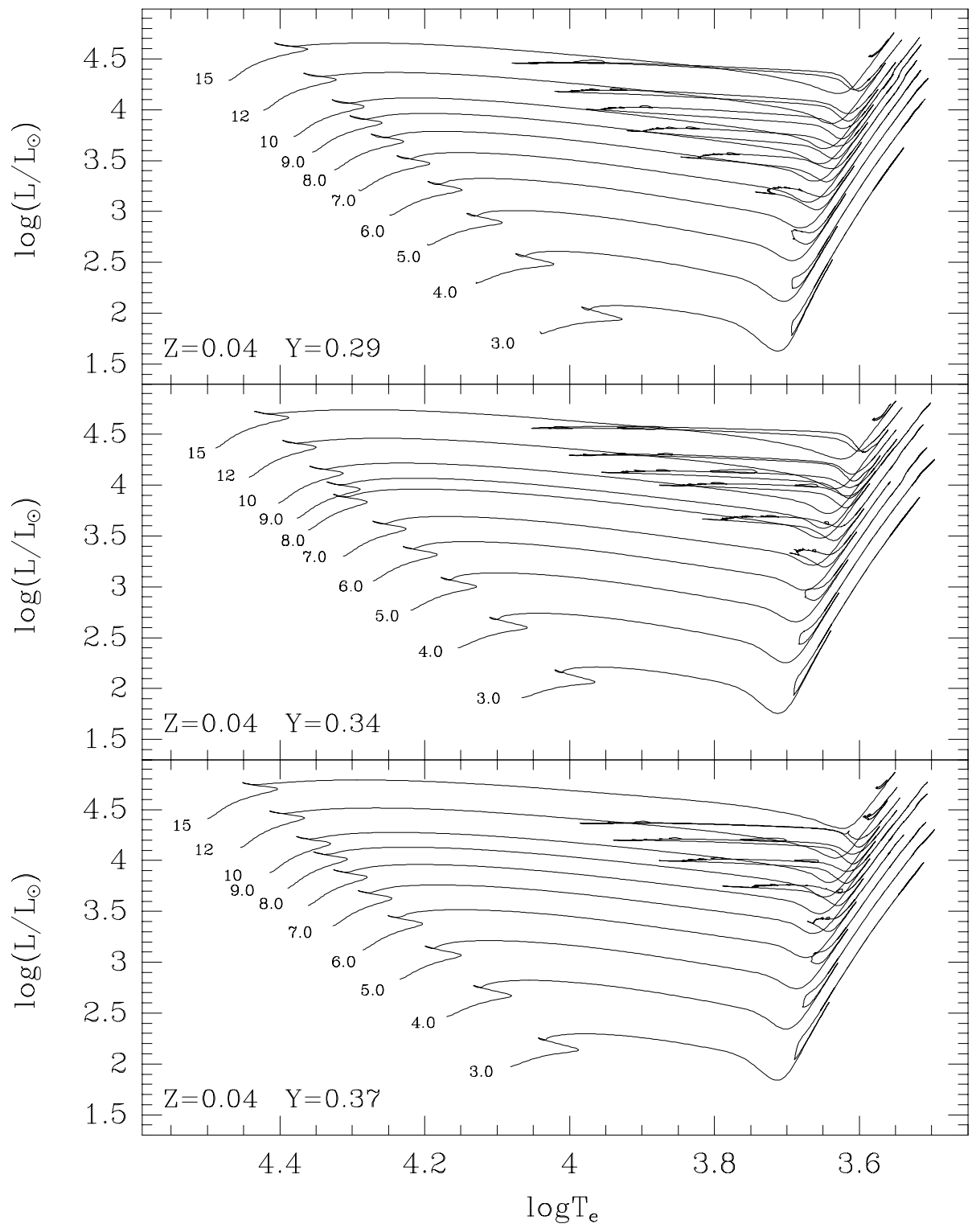
at lower metal contents were estimated by Tornambé & Chieffi (1986) and by Cassisi & Castellani (1993).

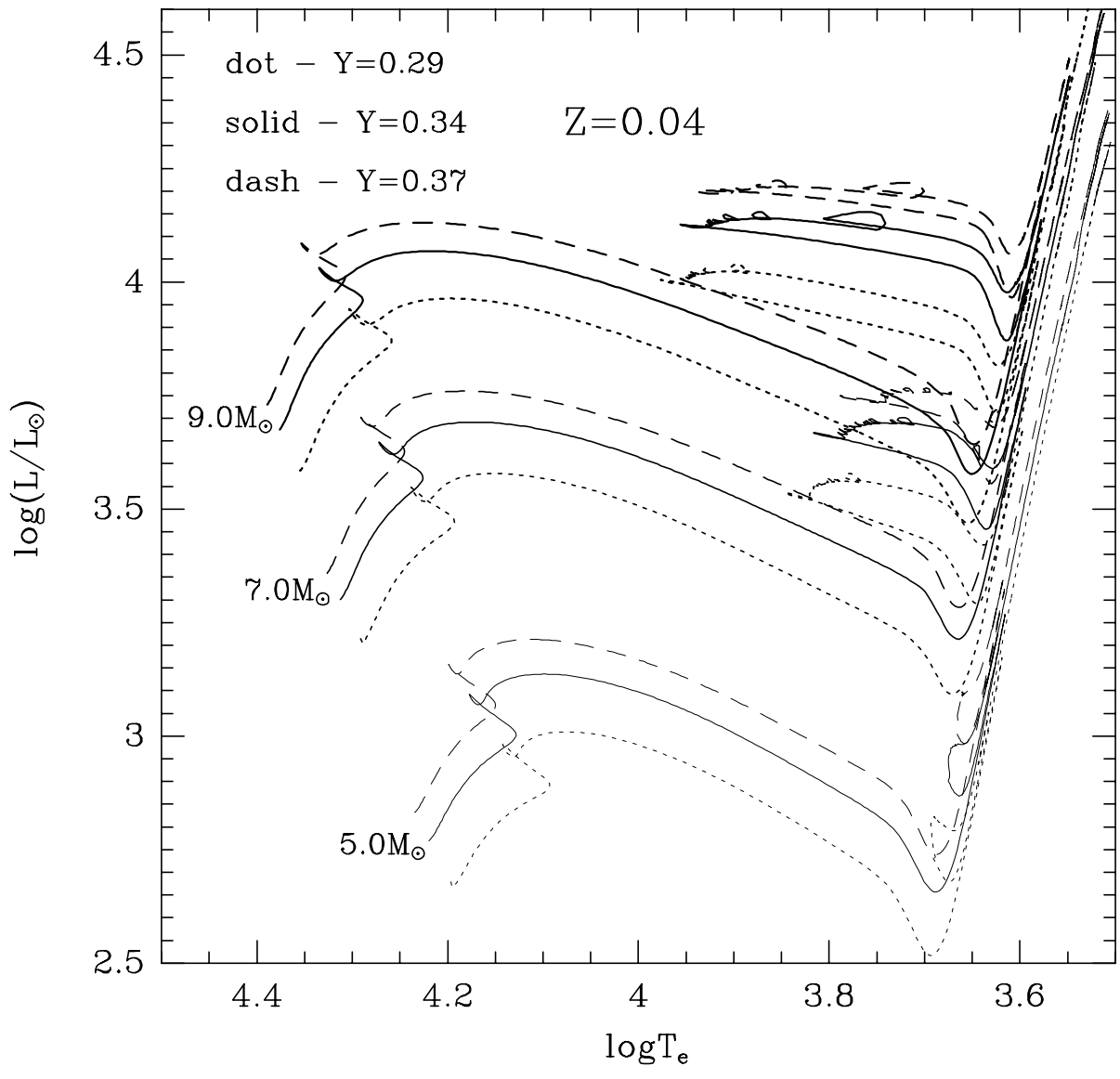
Fig. 10.— Time ratio between the 1st (circles), the 2nd (triangles), and the 3rd (squares) crossing time and the total time spent inside the instability strip as a function of stellar mass. The three panels refer to models constructed by adopting different chemical compositions.

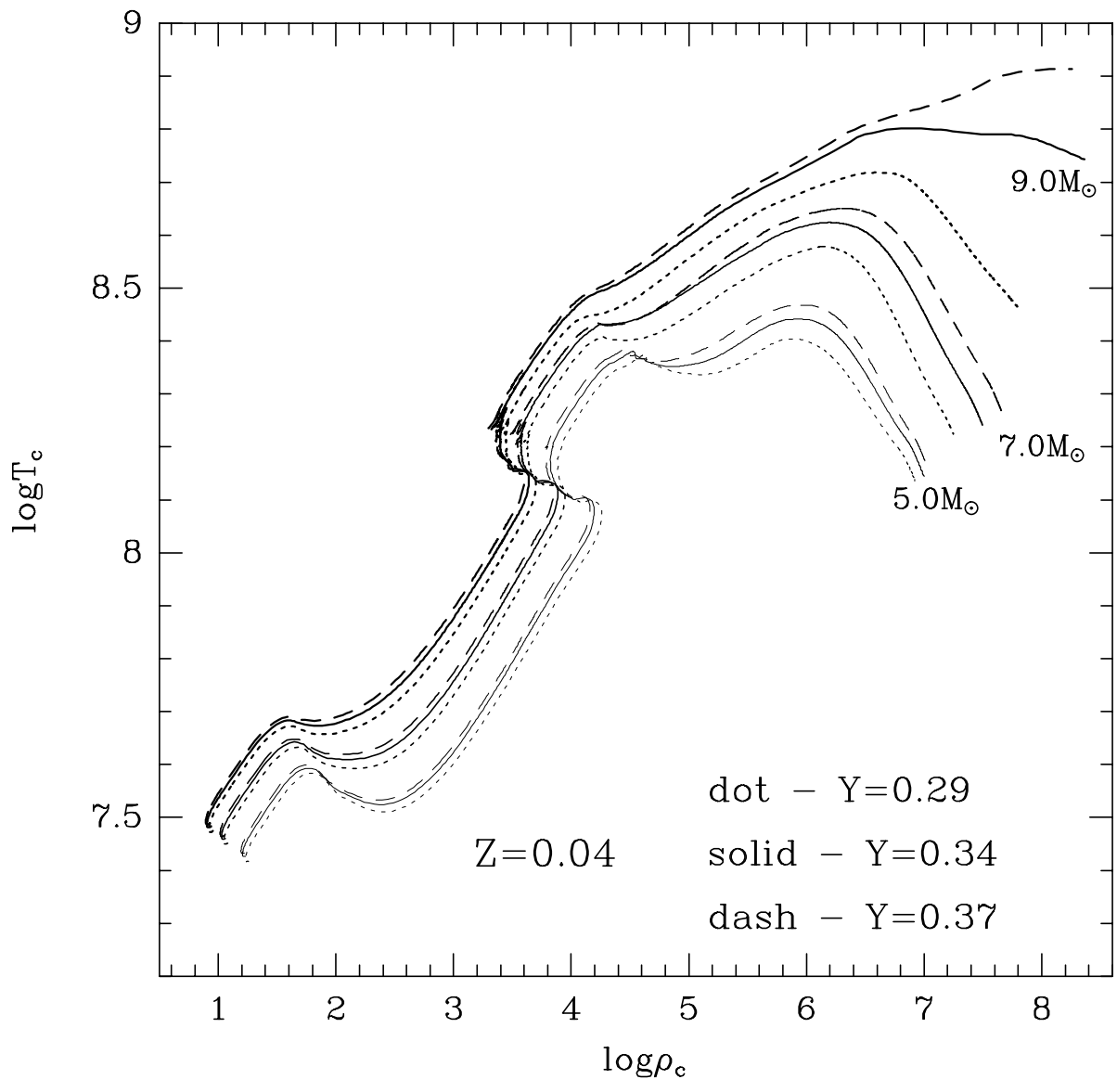


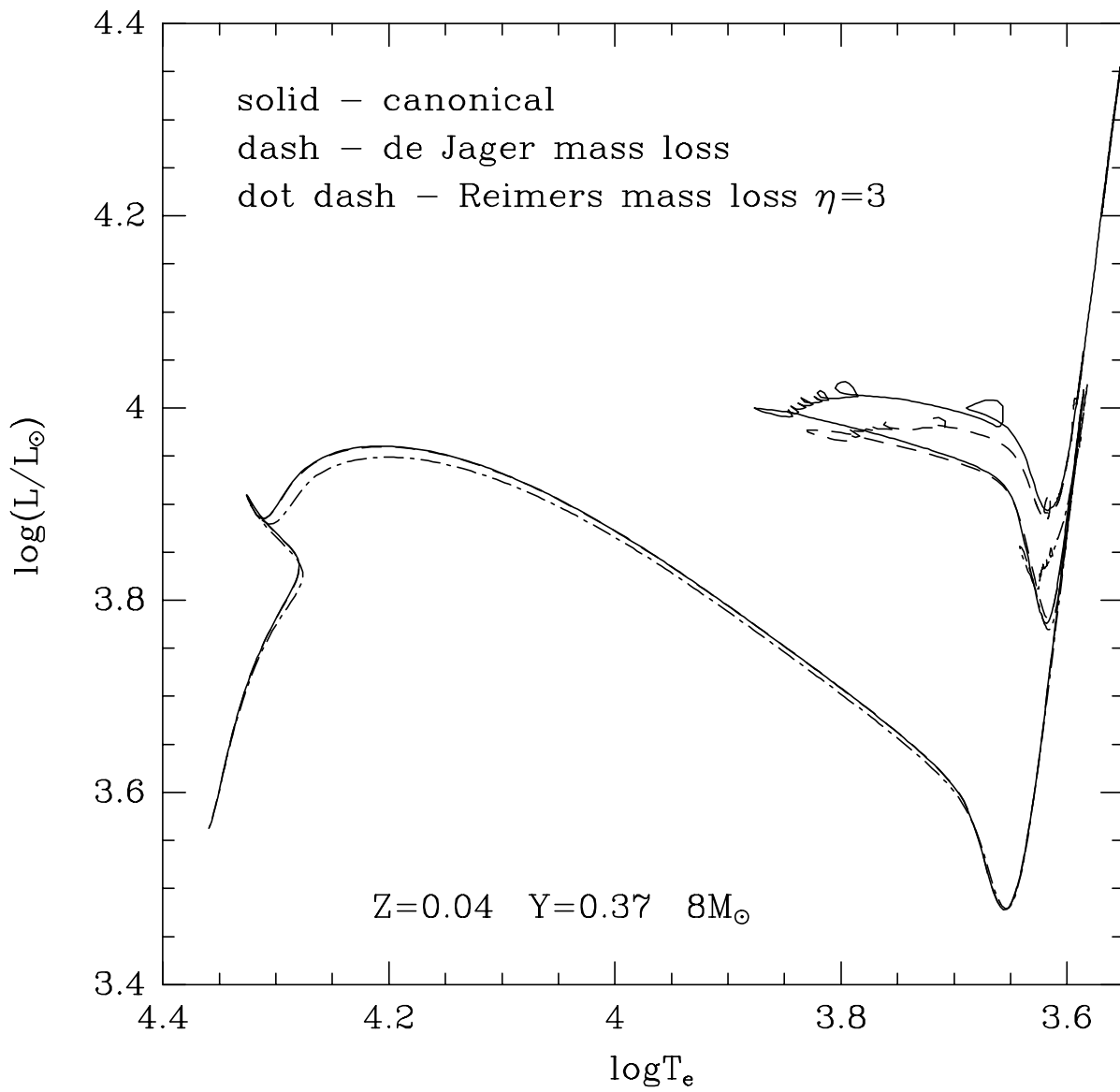


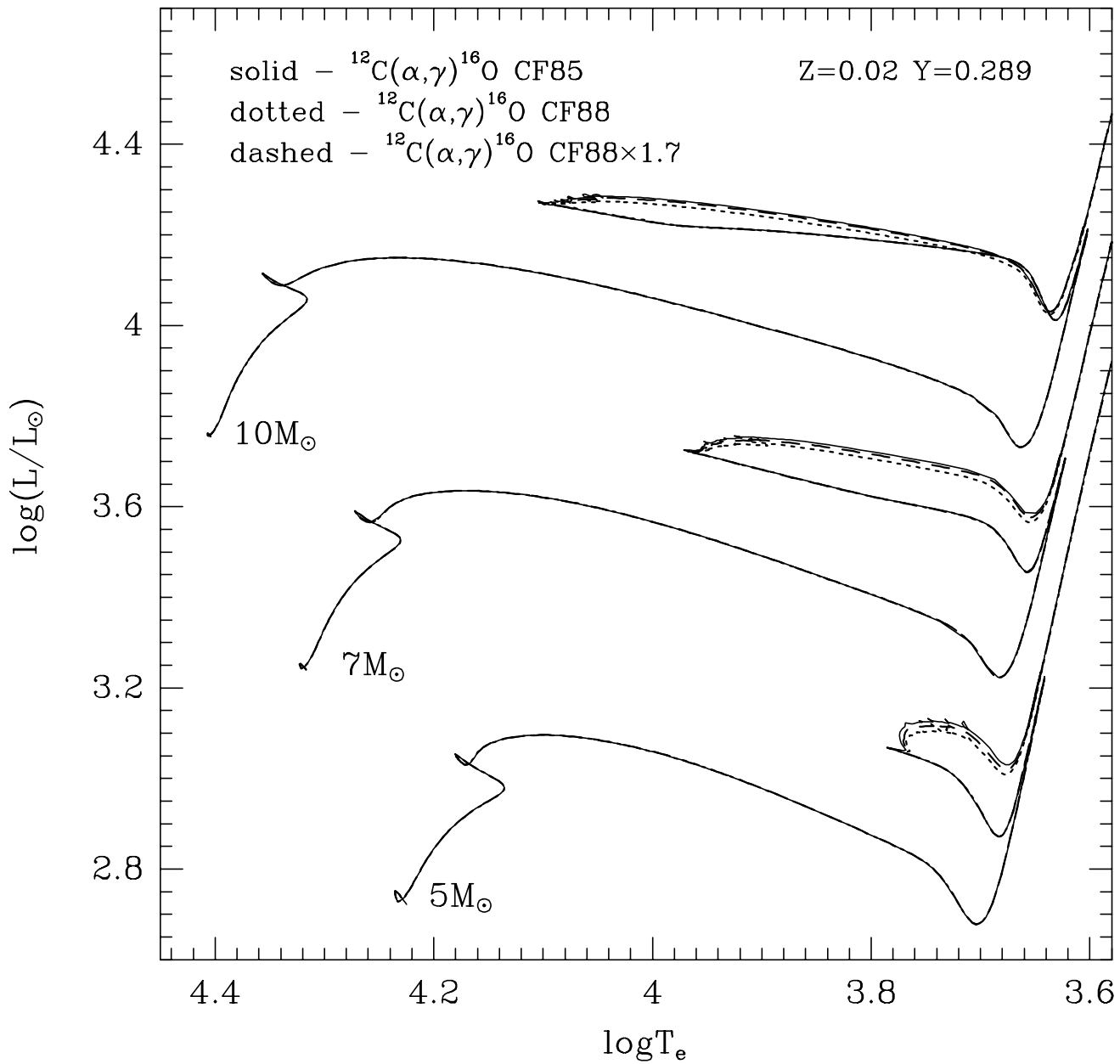


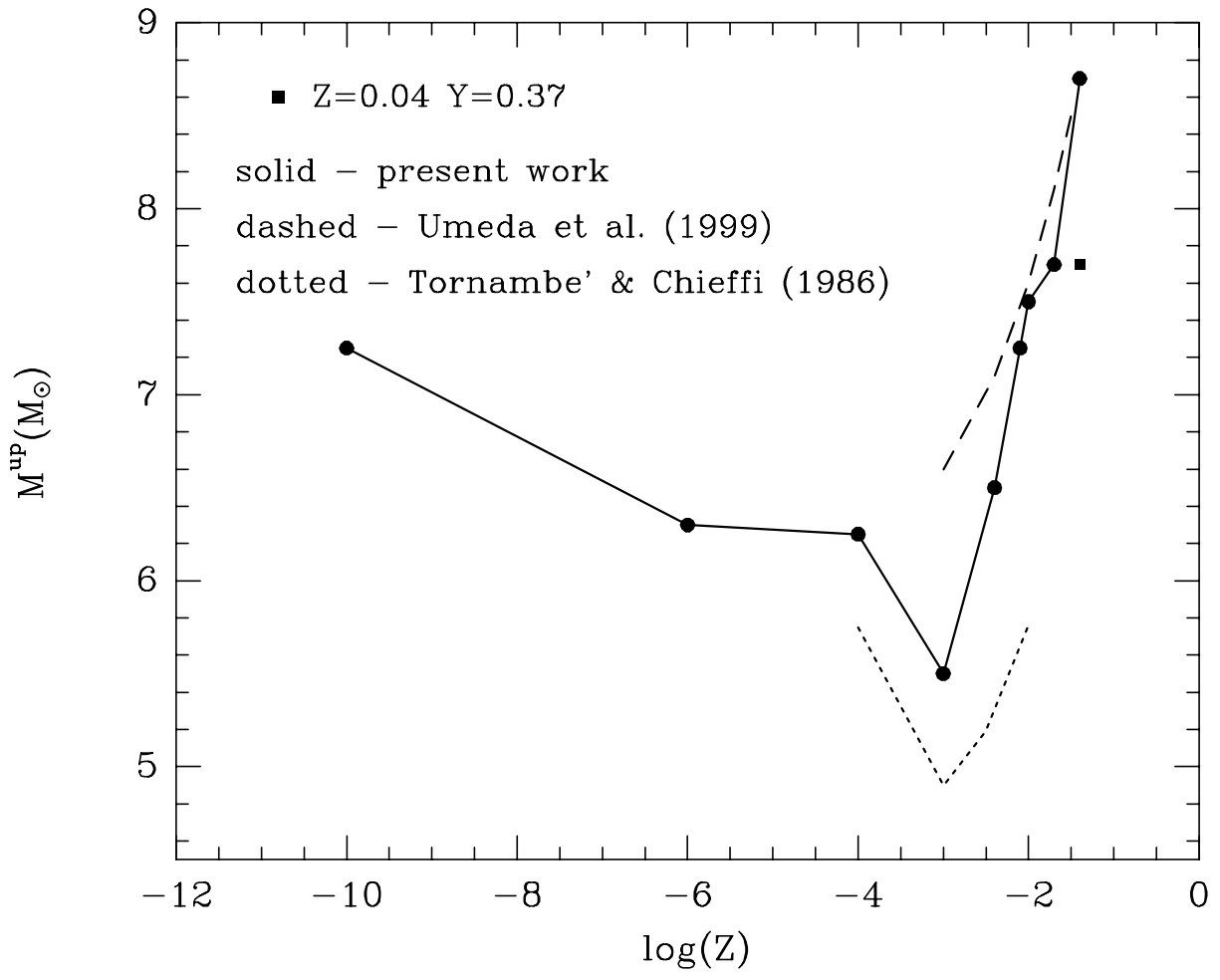












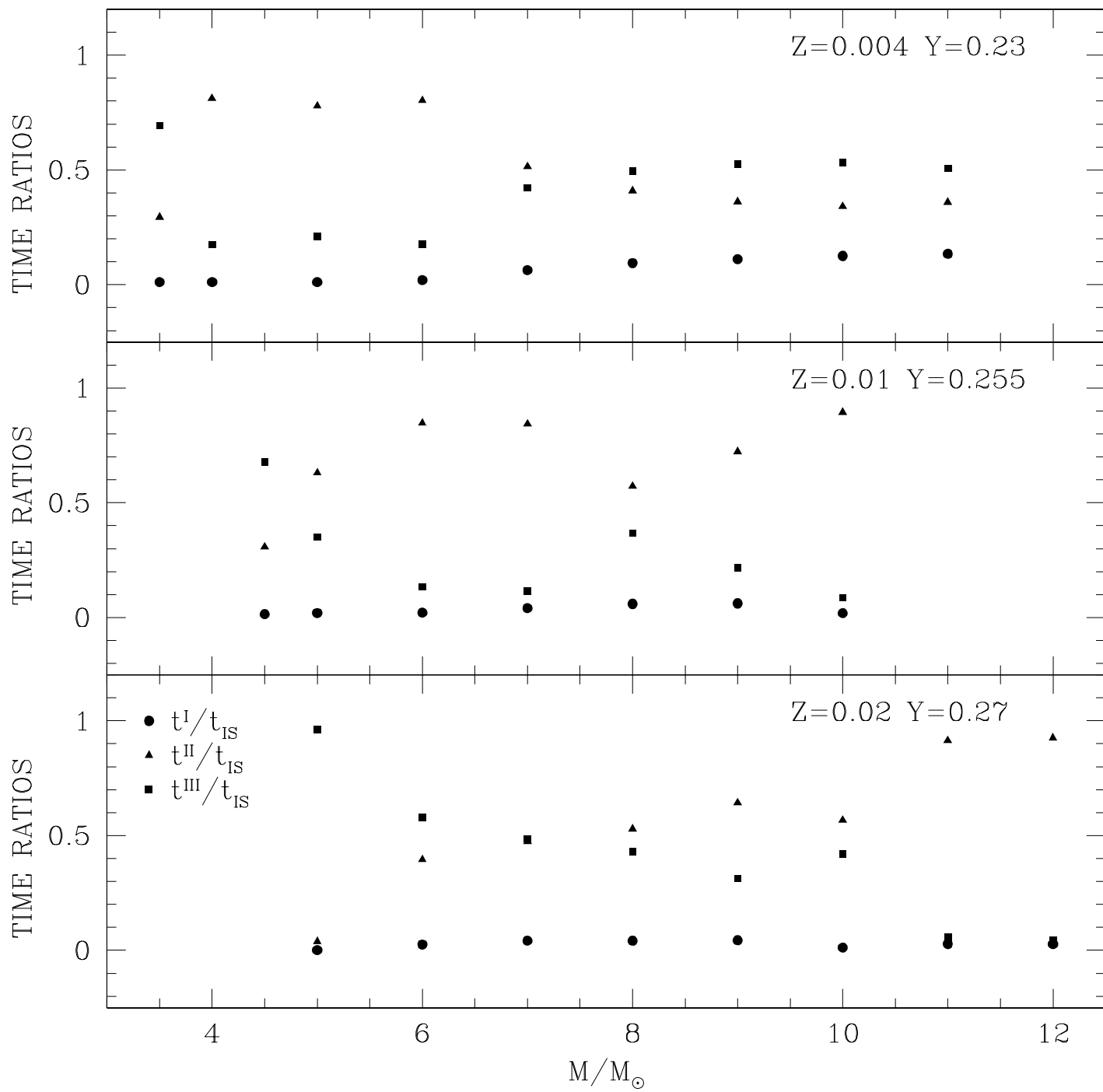


TABLE 1
SELECTED QUANTITIES FOR EVOLUTIONARY MODELS WITH $Z=0.004$.

M^a (1)	M_{cc}^b (2)	M_{He}^c (3)	τ_H^d (4)	M_{He}^e (5)	M_{cc}^f (6)	M_{He}^g (7)	M_{CO}^h (8)	τ_{He}^i (9)	$(M_{CO}^{2nd})^j$ (10)	$(\log L^{2nd})^k$ (11)	$(\log T_e^b)^l$ (12)	$(\log L^b)^m$ (13)
Y=0.23												
3.0	0.693	0.318	279.5	0.380	0.162	0.648	0.375	97.5	<i>no dredge up</i>		3.756	2.281
3.5	0.836	0.369	193.1	0.438	0.156	0.765	0.392	55.3	<i>no dredge up</i>		3.847	2.671
4.0	0.990	0.429	141.6	0.502	0.168	0.886	0.441	37.0	0.841	4.276	3.846	2.929
5.0	1.384	0.546	85.9	0.632	0.194	1.032	0.527	19.6	0.892	4.348	3.843	3.257
6.0	1.770	0.676	46.8	0.775	0.245	1.393	0.635	11.7	0.952	4.437	3.916	3.548
7.0	2.192	0.842	43.2	0.939	0.299	1.681	0.788	7.8	1.046	4.511	3.956	3.788
8.0	2.592	1.012	33.7	1.119	0.352	1.986	0.976	5.7	1.171	4.628	3.983	3.979
9.0	3.080	1.230	27.3	1.310	0.402	2.285	1.130	4.3	<i>no dredge up</i>		4.022	4.128
10.0	3.568	1.410	22.9	1.515	0.430	2.577	1.264	3.3	<i>no dredge up</i>		4.034	4.271
11.0	4.085	1.666	19.6	1.752	0.494	2.884	1.485	2.7	<i>no dredge up</i>		4.047	4.383
12.0	4.632	1.899	17.1	1.969	0.523	3.096	1.642	2.2	<i>no dredge up</i>		3.623	4.357
Y=0.27												
3.0	0.693	0.335	230.3	0.398	0.156	0.698	0.403	78.7	<i>no dredge up</i>		3.757	2.519
3.5	0.867	0.389	159.4	0.462	0.160	0.820	0.412	46.4	<i>no dredge up</i>		3.846	2.822
4.0	1.029	0.485	117.2	0.528	0.176	0.950	0.484	31.9	0.866	4.192	3.836	3.035
5.0	1.216	0.563	71.4	0.666	0.208	1.216	0.556	16.8	0.909	4.380	3.909	3.382
6.0	1.770	0.719	49.1	0.823	0.256	1.504	0.683	10.2	0.983	4.463	3.967	3.654
7.0	2.218	0.890	36.5	1.002	0.314	1.808	0.836	6.8	1.086	4.571	4.013	3.880
8.0	2.622	1.079	28.6	1.192	0.388	2.128	1.017	4.9	1.220	4.693	4.044	4.065
9.0	3.080	1.310	23.3	1.398	0.413	2.452	1.199	3.7	<i>no dredge up</i>		4.071	4.219
10.0	3.568	1.515	19.6	1.614	0.449	2.782	1.410	3.0	<i>no dredge up</i>		4.086	4.346
11.0	4.085	1.765	16.8	1.860	0.515	3.110	1.603	2.4	<i>no dredge up</i>		4.099	4.459
12.0	4.631	2.029	14.8	2.112	0.546	3.451	1.842	2.0	<i>no dredge up</i>		4.111	4.560

^a Stellar mass (solar units). ^b Mass of the convective core at the beginning of the central H-burning (M_\odot). ^c He-core mass at the end of the central H-burning (M_\odot). ^d Central H-burning lifetime (Myr). ^e He-core mass at the ignition of He-burning (M_\odot). ^f Maximum extension in mass of the convective core during central He-burning (M_\odot). ^g He-core mass at the exhaustion of central He (M_\odot). ^h CO-core mass at the exhaustion of central He (M_\odot). ⁱ Central He-burning lifetime (Myr). ^j CO-core mass at the 2^{nd} dredge up (M_\odot). ^k Surface luminosity at the 2^{nd} dredge up. ^l Blue Tip effective temperature. ^m Blue Tip surface luminosity.

TABLE 2
SELECTED QUANTITIES FOR EVOLUTIONARY MODELS WITH Z=0.01.

M^a	M_{cc}^b	M_{He}^c	τ_H^d	M_{He}^e	M_{cc}^f	M_{He}^g	M_{CO}^h	τ_{He}^i	$(M_{CO}^{2nd})^j$	$(\log L^{2nd})^k$	$(\log T_e^b)^l$	$(\log L^b)^m$
(1)	(2)	(3)	(4)	(5)	(6)	(7)	(8)	(9)	(10)	(11)	(12)	(13)
Y=0.23												
3.0	0.619	0.299	333.6	0.366	0.173	0.548	0.256	147.3	<i>no dredge up</i>		3.730	2.033
4.0	0.924	0.404	162.0	0.481	0.164	0.777	0.388	46.2	<i>no dredge up</i>		3.779	2.684
4.5	1.075	0.469	122.1	0.545	0.173	0.906	0.439	30.8	0.833	4.259	3.854	2.897
5.0	1.286	0.602	95.6	0.611	0.192	1.032	0.508	21.8	0.862	4.307	3.904	3.123
6.0	1.660	0.649	64.0	0.755	0.232	1.291	0.583	12.6	0.919	4.376	3.904	3.440
7.0	2.065	0.815	46.4	0.914	0.287	1.569	0.720	8.3	0.997	4.462	3.965	3.695
8.0	2.418	1.002	35.6	1.087	0.342	1.836	0.849	5.8	1.093	4.543	3.969	3.879
9.0	2.943	1.194	28.6	1.280	0.412	2.115	1.013	4.3	1.207	4.723	3.972	4.040
10.0	3.386	1.403	23.7	1.488	0.505	2.414	1.185	3.4	<i>no dredge up</i>		4.003	4.190
11.0	3.885	1.604	20.2	1.708	0.563	2.641	1.356	2.7	<i>no dredge up</i>		3.944	4.138
12.0	4.457	1.852	17.5	1.940	0.581	2.966	1.606	2.2	<i>no dredge up</i>		3.635	4.251
Y=0.255												
3.0	0.634	0.328	296.2	0.376	0.166	0.584	0.364	136.1	<i>no dredge up</i>		3.728	2.083
4.0	0.924	0.466	145.3	0.497	0.170	0.830	0.452	42.6	0.776	4.120	3.771	2.749
4.5	1.114	0.485	108.5	0.563	0.182	0.948	0.447	27.3	0.844	4.278	3.853	2.982
5.0	1.250	0.558	85.4	0.634	0.199	1.095	0.556	20.6	0.874	4.326	3.889	3.198
6.0	1.660	0.734	57.7	0.784	0.243	1.368	0.676	12.3	0.933	4.400	3.902	3.507
7.0	2.064	0.879	41.8	0.947	0.303	1.650	0.816	7.9	1.025	4.495	3.961	3.760
8.0	2.476	1.035	32.1	1.134	0.350	1.910	0.885	5.4	1.134	4.599	3.956	3.938
9.0	2.949	1.258	25.8	1.335	0.435	2.242	1.168	4.3	<i>no dredge up</i>		4.001	4.106
10.0	3.423	1.475	21.5	1.548	0.516	2.500	1.249	3.1	<i>no dredge up</i>		3.979	4.233
11.0	3.965	1.708	18.3	1.788	0.531	2.760	1.417	2.6	<i>no dredge up</i>		3.640	4.195
12.0	4.500	1.945	15.9	2.034	0.601	3.111	1.754	2.2	<i>no dredge up</i>		3.633	4.305
Y=0.27												
3.0	0.634	0.332	273.5	0.382	0.163	0.590	0.380	119.6	<i>no dredge up</i>		3.727	2.140
4.0	0.955	0.412	133.2	0.509	0.169	0.845	0.422	38.1	0.792	4.182	3.774	2.783
4.5	1.114	0.492	100.8	0.576	0.186	0.976	0.466	25.6	0.849	4.293	3.852	3.033
5.0	1.286	0.558	79.4	0.650	0.200	1.111	0.507	18.5	0.880	4.334	3.886	3.252
6.0	1.660	0.734	53.7	0.805	0.245	1.380	0.618	11.0	0.942	4.408	3.880	3.533
7.0	2.064	0.883	38.9	0.972	0.304	1.668	0.761	7.2	1.033	4.494	3.937	3.780
8.0	2.476	1.072	30.1	1.159	0.375	1.973	0.947	5.2	1.152	4.571	3.959	3.975
9.0	2.982	1.277	24.3	1.363	0.458	2.276	1.090	3.9	<i>no dredge up</i>		3.980	4.134
10.0	3.459	1.488	20.2	1.592	0.538	2.555	1.249	3.0	<i>no dredge up</i>		3.971	4.261
11.0	3.965	1.752	17.2	1.817	0.557	2.834	1.495	2.5	<i>no dredge up</i>		3.640	4.234
12.0	4.500	2.011	15.1	2.085	0.601	3.184	1.793	2.1	<i>no dredge up</i>		3.633	4.344

^a Stellar mass (solar units). ^b Mass of the convective core at the beginning of the central H-burning (M_\odot). ^c He-core mass at the end of the central H-burning (M_\odot). ^d Central H-burning lifetime (Myr). ^e He-core mass at the ignition of He-burning (M_\odot). ^f Maximum extension in mass of the convective core during central He-burning (M_\odot). ^g He-core mass at the exhaustion of central He (M_\odot). ^h CO-core mass at the exhaustion of central He (M_\odot). ⁱ Central He-burning lifetime (Myr). ^j CO-core mass at the 2nd dredge up (M_\odot). ^k Surface luminosity at the 2nd dredge up. ^l Blue Tip effective temperature. ^m Blue Tip surface luminosity.

TABLE 3
SELECTED QUANTITIES FOR EVOLUTIONARY MODELS WITH Z=0.02.

M^a	M_{cc}^b	M_{He}^c	τ_H^d	M_{He}^e	M_{cc}^f	M_{He}^g	M_{CO}^h	τ_{He}^i	$(M_{CO}^{2nd})^j$	$(\log L^{2nd})^k$	$(\log T_e^b)^l$	$(\log L^b)^m$
(1)	(2)	(3)	(4)	(5)	(6)	(7)	(8)	(9)	(10)	(11)	(12)	(13)
Y=0.27												
3.0	0.590	0.315	349.9	0.378	0.171	0.559	0.379	160.0	<i>no dredge up</i>		3.712	1.931
4.0	0.884	0.450	164.2	0.502	0.176	0.749	0.402	51.9	<i>no dredge up</i>		3.719	2.516
4.5	1.075	0.509	121.7	0.570	0.198	0.883	0.448	32.0	0.821	4.228	3.732	2.732
5.0	1.238	0.553	94.1	0.643	0.209	1.027	0.512	22.0	0.856	4.302	3.780	3.038
6.0	1.602	0.696	61.4	0.795	0.250	1.305	0.618	12.0	0.925	4.399	3.885	3.399
7.0	2.005	0.866	43.6	0.962	0.299	1.600	0.819	8.1	0.998	4.400	3.974	3.674
8.0	2.418	1.035	33.0	1.138	0.365	1.894	0.953	5.7	1.096	4.591	4.029	3.894
9.0	2.917	1.242	26.1	1.280	0.435	2.200	1.136	4.3	<i>no dredge up</i>		4.040	4.092
10.0	3.386	1.475	21.5	1.558	0.524	2.505	1.282	3.3	<i>no dredge up</i>		4.104	4.228
11.0	3.885	1.715	18.1	1.794	0.661	2.830	1.485	2.6	<i>no dredge up</i>		4.132	4.360
12.0	4.413	1.964	15.7	2.050	0.733	3.176	1.806	2.2	<i>no dredge up</i>		4.143	4.482
Y=0.289												
3.0	0.504	0.334	316.5	0.387	0.169	0.578	0.378	140.2	<i>no dredge up</i>		3.711	1.967
4.0	0.901	0.453	148.2	0.516	0.184	0.781	0.441	46.2	<i>no dredge up</i>		3.715	2.577
5.0	1.238	0.589	85.7	0.663	0.208	1.074	0.534	20.0	0.870	4.324	3.749	3.132
5.5	1.415	0.652	68.4	0.738	0.234	1.216	0.601	14.4	0.904	4.370	3.848	3.280
6.0	1.602	0.711	56.0	0.821	0.245	1.361	0.664	11.1	0.944	4.422	3.900	3.454
6.5	1.799	0.804	46.8	0.902	0.282	1.517	0.783	9.2	1.005	4.424	3.937	3.598
7.0	2.005	0.884	39.9	0.992	0.313	1.654	0.802	7.4	1.052	4.535	3.971	3.725
7.5	2.267	0.970	34.5	1.081	0.348	1.814	0.932	6.3	1.112	4.590	4.002	3.838
8.0	2.505	1.079	30.2	1.181	0.381	1.962	0.967	5.3	1.173	4.631	4.025	3.942
9.0	2.917	1.312	24.0	1.381	0.444	2.289	1.200	4.1	<i>no dredge up</i>		4.069	4.123
10.0	3.423	1.559	19.8	1.611	0.538	2.602	1.359	3.1	<i>no dredge up</i>		4.104	4.270
12.0	4.457	2.074	14.6	2.117	0.784	3.278	1.778	2.0	<i>no dredge up</i>		4.155	4.517
13.0	5.058	2.310	12.9	2.398	0.980	3.647	2.121	1.8	<i>no dredge up</i>		4.170	4.617
14.0	5.607	2.627	11.6	2.664	0.975	4.015	2.481	1.6	<i>no dredge up</i>		4.174	4.708

^a Stellar mass (solar units). ^b Mass of the convective core at the beginning of the central H-burning (M_\odot). ^c He-core mass at the end of the central H-burning (M_\odot). ^d Central H-burning lifetime (Myr). ^e He-core mass at the ignition of He-burning (M_\odot). ^f Maximum extension in mass of the convective core during central He-burning (M_\odot). ^g He-core mass at the exhaustion of central He (M_\odot). ^h CO-core mass at the exhaustion of central He (M_\odot). ⁱ Central He-burning lifetime (Myr). ^j CO-core mass at the 2nd dredge up (M_\odot). ^k Surface luminosity at the 2nd dredge up. ^l Blue Tip effective temperature. ^m Blue Tip surface luminosity.

TABLE 4
SELECTED QUANTITIES FOR EVOLUTIONARY MODELS WITH Z=0.04.

M^a (1)	M_{cc}^b (2)	M_{He}^c (3)	τ_H^d (4)	M_{He}^e (5)	M_{cc}^f (6)	M_{He}^g (7)	M_{CO}^h (8)	τ_{He}^i (9)	$(M_{CO}^{2nd})^j$ (10)	$(\log L^{2nd})^k$ (11)	$(\log T_e^b)^l$ (12)	$(\log L^b)^m$ (13)
Y=0.29												
3.0	0.518	0.312	367.6	0.369	0.173	0.517	0.264	165.8	<i>no dredge up</i>		3.694	1.854
3.5	0.666	0.374	237.9	0.430	0.154	0.596	0.292	95.1	<i>no dredge up</i>		3.694	2.071
4.0	0.786	0.435	165.4	0.498	0.168	0.686	0.322	56.2	<i>no dredge up</i>		3.693	2.307
5.0	1.104	0.569	92.7	0.645	0.199	0.927	0.449	25.4	0.844	4.206	3.694	2.807
6.0	1.433	0.722	59.3	0.805	0.250	1.198	0.556	13.3	0.890	4.350	3.743	3.191
7.0	1.869	0.878	41.4	0.978	0.311	1.485	0.685	8.1	0.973	4.463	3.846	3.535
8.0	2.292	1.071	30.9	1.166	0.365	1.785	0.843	5.7	1.056	4.543	3.921	3.794
9.0	2.720	1.267	24.3	1.382	0.454	2.100	1.019	4.2	1.216	4.714	3.977	4.004
10.0	3.277	1.527	19.9	1.612	0.538	2.434	1.233	3.2	<i>no dredge up</i>		4.020	4.180
12.0	4.282	2.065	14.5	2.137	0.769	3.145	1.911	2.2	<i>no dredge up</i>		4.079	4.458
15.0	5.953	2.996	10.3	3.043	0.927	4.115	2.512	1.3	<i>no dredge up</i>		3.587	4.518
Y=0.34												
3.0	0.548	0.339	264.9	0.393	0.159	0.593	0.386	125.3	<i>no dredge up</i>		3.690	1.942
3.5	0.666	0.399	172.2	0.462	0.162	0.677	0.389	72.6	<i>no dredge up</i>		3.688	2.181
4.0	0.825	0.458	120.5	0.538	0.174	0.783	0.403	43.4	<i>no dredge up</i>		3.683	2.460
4.5	0.972	0.524	86.0	0.617	0.194	0.905	0.434	27.5	0.802	4.190	3.678	2.676
5.0	1.126	0.602	68.3	0.699	0.213	1.038	0.488	18.8	0.842	4.271	3.675	2.909
5.5	1.314	0.680	54.4	0.785	0.244	1.178	0.541	13.7	0.883	4.344	3.677	3.154
6.0	1.544	0.773	43.6	0.875	0.271	1.327	0.618	10.2	0.931	4.415	3.687	3.346
6.5	1.736	0.866	37.1	0.967	0.303	1.483	0.694	8.1	0.973	4.459	3.760	3.513
7.0	1.937	0.965	31.4	1.065	0.331	1.651	0.815	6.8	1.050	4.538	3.816	3.668
8.0	2.418	1.258	20.3	1.346	0.435	2.105	1.056	4.3	1.238	4.750	3.876	4.000
8.5	2.631	1.287	20.0	1.393	0.456	2.150	1.072	4.0	1.247	4.783	3.930	4.029
9.0	2.949	1.411	18.3	1.514	0.492	2.340	1.293	3.6	<i>no dredge up</i>		3.956	4.126
10.0	3.386	1.670	15.6	1.776	0.603	2.684	1.388	2.7	<i>no dredge up</i>		4.000	4.294
12.0	4.413	2.252	11.7	2.355	0.901	3.456	1.819	1.9	<i>no dredge up</i>		4.052	4.559
15.0	6.172	3.281	8.5	3.345	1.050	4.540	2.941	1.2	<i>no dredge up</i>		3.582	4.643
Y=0.37												
3.0	0.559	0.349	220.3	0.411	0.153	0.635	0.391	102.5	<i>no dredge up</i>		3.689	2.055
3.5	0.688	0.424	142.1	0.486	0.162	0.731	0.414	58.3	<i>no dredge up</i>		3.685	2.302
4.0	0.825	0.489	100.5	0.567	0.183	0.849	0.445	35.7	0.782	4.149	3.678	2.562
4.5	0.994	0.566	75.1	0.648	0.197	0.978	0.479	23.4	0.824	4.235	3.672	2798
5.0	1.556	0.647	56.3	0.733	0.219	1.114	0.522	16.1	0.882	4.273	3.667	3.010
5.5	1.362	0.723	46.0	0.823	0.250	1.257	0.590	11.9	0.903	4.381	3.664	3.203
6.0	1.544	0.824	36.4	0.917	0.268	1.418	0.706	9.2	0.963	4.420	3.662	3.406
6.5	1.799	0.908	30.7	1.014	0.316	1.577	0.798	7.4	1.020	4.468	3.717	3.590
7.0	2.005	1.026	26.0	1.119	0.353	1.751	0.937	6.1	1.093	4.553	3.788	3.750
7.5	2.148	1.128	22.6	1.229	0.393	1.925	1.007	4.9	1.161	4.668	3.836	3.882
8.0	2.418	1.222	20.0	1.346	0.435	2.105	1.056	4.3	1.236	4.767	3.877	4.000
9.0	2.917	1.549	16.0	1.599	0.528	2.479	1.355	3.2	<i>no dredge up</i>		3.940	4.198
10.0	3.423	1.799	13.3	1.870	0.649	2.857	1.725	2.6	<i>no dredge up</i>		3.982	4.366
12.0	4.500	2.429	9.9	2.489	0.930	3.516	1.875	1.7	<i>no dredge up</i>		3.594	4.429
15.0	6.281	3.499	7.6	3.525	1.114	4.870	3.015	1.0	<i>no dredge up</i>		3.576	4.713

^a Stellar mass (solar units). ^b Mass of the convective core at the beginning of the central H-burning (M_\odot). ^c He-core mass at the end of the central H-burning (M_\odot). ^d Central H-burning lifetime (Myr). ^e He-core mass at the ignition of He-burning (M_\odot). ^f Maximum extension in mass of the convective core during central He-burning (M_\odot). ^g He-core mass at the exhaustion of central He (M_\odot). ^h CO-core mass at the exhaustion of central He (M_\odot). ⁱ Central He-burning lifetime (Myr). ^j CO-core mass at the 2nd dredge up (M_\odot). ^k Surface luminosity at the 2nd dredge up. ^l Blue Tip effective temperature. ^m Blue Tip surface luminosity.

TABLE 5
ANALYTICAL RELATIONS $-\log M = \alpha + \beta \log L + \gamma \log T_e$ FOR BOTH ZAMS AND OC PHASES.

$Y - Z^a$	ZAMS				OC			
	α^b	β^b	γ^b	r^c	α	β	γ	r
0.255 — 0.01	9.901	+0.73	-2.63	0.999	9.296	+0.693	-2.55	0.999
...	± 0.003	± 0.05	± 0.30	...	± 0.002	± 0.031	± 0.19	...
0.289 — 0.02	8.790	+0.69	-2.30	0.999	7.341	+0.620	-2.05	0.999
...	± 0.002	± 0.03	± 0.20	...	± 0.001	± 0.013	± 0.08	...
0.34 — 0.04	13.151	+0.89	-3.54	0.999	7.040	+0.590	-1.96	0.999
...	± 0.002	± 0.03	± 0.18	...	± 0.003	± 0.02	± 0.13	...
0.37 — 0.04	14.2008	+0.942	-3.82	0.999	8.134	+0.642	-2.27	0.999
...	± 0.0004	± 0.009	± 0.05	...	± 0.002	± 0.017	± 0.11	...

^aAbundances in mass for the adopted He and metal contents.

^bNumerical coefficients connecting the stellar mass (solar units) to the luminosity (solar units) and to the effective temperature (K).

^cCorrelation coefficient.

TABLE 6
DEPENDENCE OF SELECTED PARAMETERS ON THE $^{12}\text{C}(\alpha, \gamma)^{16}\text{O}$ NUCLEAR REACTION RATE.

NRR ^a	$M/M_\odot = 5$				$M/M_\odot = 7$				$M/M_\odot = 10$			
	τ_{He}^b	t_{IS}^c	M_{CO}^d	C/O ^e	τ_{He}	t_{IS}	M_{CO}	C/O	τ_{He}	t_{IS}	M_{CO}	C/O
CFHZ85	19.88	8.50	0.534	0.41	7.34	0.152	0.802	0.44	3.09	0.471	1.359	0.34
CF88	18.26	6.38	0.508	1.25	6.85	0.148	0.785	1.19	2.85	0.482	1.303	1.04
CF88 $\times 1.7$	19.03	7.54	0.514	0.70	7.16	0.149	0.782	0.67	3.04	0.457	1.378	0.52

^aAdopted $^{12}\text{C}(\alpha, \gamma)^{16}\text{O}$ nuclear reaction rate. See text for more details.

^bCentral He-burning lifetime (Myr).

^cTotal time spent inside the instability strip (Myr).

^dCO core mass at the He exhaustion (M_\odot).

^eCarbon/Oxygen abundance ratio.

TABLE 7
CEPHEID PROPERTIES ACROSS THE INSTABILITY STRIP

First Crossing					Second Crossing				Third Crossing			
M^a	$\log L^b$	$\log T_e^c$	$\log P^d$	t_c^e	$\log L$	$\log T_e$	$\log P$	t_c	$\log L$	$\log T_e$	$\log P$	t_c
(1)	(2)	(3)	(4)	(5)	(6)	(7)	(8)	(9)	(10)	(11)	(12)	(13)
Y=0.23 Z=0.004												
3.5	2.431	3.820	-0.1526	7.124 (4) ^f	2.635	3.807	0.0818	1.841 (6) ^f	2.729	3.804	0.1776	4.349 (6) ^f
4.0	2.620	3.808	0.0171	4.067 (4)	2.869	3.790	0.3059	2.845 (6)	2.926	3.791	0.3630	6.187 (5)
5.0	3.017	2.939	0.3026	2.105 (4)	3.192	3.770	0.5964	1.476 (6)	3.253	3.768	0.6655	3.987 (5)
6.0	3.203	3.770	0.5412	1.118 (4)	3.438	3.756	0.8089	4.467 (5)	3.522	3.752	0.9051	9.862 (4)
7.0	3.432	3.756	0.7470	6.735 (3)	3.675	3.742	1.0239	5.452 (5)	3.745	3.737	1.1005	4.457 (4)
8.0	3.625	3.743	0.9241	4.302 (3)	3.886	3.730	1.2166	1.861 (4)	3.928	3.727	1.2616	2.257 (4)
9.0	3.794	3.735	1.0672	3.230 (3)	4.069	3.720	1.3763	1.052 (4)	4.078	3.717	1.3898	1.531 (4)
10.0	3.943	3.721	1.2033	2.698 (3)	4.227	3.711	1.5138	7.364 (3)	4.205	3.713	1.4880	1.150 (4)
11.0	4.088	3.722	1.3159	2.353 (3)	4.364	3.704	1.6354	6.283 (3)	4.317	3.708	1.5745	8.860 (3)
Y=0.255 Z=0.01												
4.5	2.719	3.803	0.1012	3.870 (4)	2.923	3.786	0.3444	8.233 (5)	3.012	3.781	0.4461	1.810 (6)
5.0	2.871	3.791	0.2418	2.560 (4)	3.106	3.771	0.5272	8.037 (5)	3.188	3.766	0.6200	4.452 (5)
6.0	3.143	3.770	0.5065	1.360 (4)	3.401	3.749	0.8127	5.432 (5)	3.457	3.745	0.8745	8.454 (4)
7.0	3.374	3.754	0.7124	8.705 (3)	3.634	3.733	1.0292	1.801 (5)	3.667	3.738	1.0455	2.485 (4)
8.0	3.518	3.743	0.8405	5.506 (3)	3.780	3.722	1.1512	5.317 (4)	3.774	3.730	1.1214	3.425 (4)
9.0	3.739	3.734	1.0371	4.424 (3)	4.033	3.714	1.3782	5.211 (4)	4.013	3.720	1.3359	1.550 (4)
10.0	3.884	3.727	1.1566	4.120 (3)	4.194	3.716	1.4823	1.940 (5)	4.147	3.711	1.4546	1.890 (4)
Y=0.27 Z=0.02												
5.0	2.816	3.785	0.2141	1.051 (4)	2.990	3.775	0.4222	4.058 (5)	3.059	3.774	0.4880	1.010 (7)
6.0	3.078	3.757	0.4981	7.138 (3)	3.281	3.740	0.7413	1.100 (5)	3.385	3.732	0.8675	1.607 (5)
7.0	3.306	3.740	0.7174	6.075 (3)	3.521	3.719	0.9822	6.884 (4)	3.623	3.712	1.1016	7.045 (4)
8.0	3.494	3.724	0.8976	3.822 (3)	3.735	3.706	1.1818	4.851 (4)	3.816	3.703	1.2666	3.933 (4)
9.0	3.662	3.716	1.0400	3.628 (3)	3.931	3.698	1.3496	5.329 (4)	3.976	3.695	1.4004	2.599 (4)
10.0	3.804	3.710	1.1579	3.471 (3)	3.963	3.642	1.5202	1.643 (5)	4.100	3.690	1.4985	1.218 (5)
11.0	3.915	3.695	1.2783	3.989 (4)	4.195	3.648	1.6889	1.317 (6)	4.113	3.654	1.5928	8.403 (4)
12.0	4.012	3.683	1.3773	3.454 (4)	4.328	3.641	1.8053	1.175 (6)	4.207	3.652	1.6597	5.931 (4)

^a Stellar mass (solar units).

^b Luminosity (solar units).

^c Effective temperature (K).

^d Period (day).

^e Crossing time (yr).

^f Numbers in parentheses are powers of 10.